Supporting information for:

From Borane to Metal-Bound Boraindene: A Cascade of Bond-Breaking and -Making at Rhodium

Emily J. Addison,[a] Joseph A. Zurakowski,[a] Paul D. Boyle,[a]
David J. Nelson,*[,b] and Marcus W. Drover*[,a]

*E-mails: david.nelson@strath.ac.uk, marcus.drover@uwo.ca

[a]Department of Chemistry, Western University, 1151 Richmond Street, London, ON, N8K 3G6, Canada
[b]Department of Pure and Applied Chemistry, University of Strathclyde, 295 Cathedral Street, Glasgow, G1 1XL, United Kingdom

1. Experimental Section:

General considerations. All experiments were carried out employing standard Schlenk techniques under an atmosphere of dry nitrogen employing degassed, dried solvents. Non-halogenated solvents were tested with a standard purple solution of sodium benzophenone ketyl in tetrahydrofuran to confirm effective moisture removal. d_6-benzene was dried over molecular sieves and degassed by three freeze-pump-thaw cycles. [Cp*Rh(NBD)][1] and $\{HB(C_6F_5)_2\}_2$[2] were prepared using literature procedures - $\{DB(C_6F_5)_2\}_2$ was compared by analogy to $\{HB(C_6F_5)_2\}_2$ using D-$SiEt_3$ purchased from Sigma Aldrich. All other reagents were purchased from commercial vendors and used without further purification unless otherwise stated.

Physical methods. All NMR data were recorded with a Bruker AVIII HD 400 MHz or a Bruker Neo 600 MHz instrument. ^{1}H NMR spectra are reported in parts per million (ppm) and are referenced to residual solvent e.g., $^1H(C_6D_6)$: $\delta = 7.16$; $^{13}C(C_6D_6)$: $\delta = 128.06$; coupling constants are reported in Hz. ^{13}C and ^{31}P NMR spectra were performed as proton-decoupled experiments (unless explicitly stated otherwise) and are reported in ppm. n.o. = not observed. Mass spectrometry was carried out with a Thermo Scientific Orbitrap Exploris 120 instrument.

2. Preparation of Compounds:

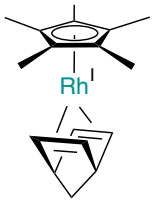

[Cp*Rh(NBD)][1] (**1**; $C_{21}H_{23}Rh$, Mw = 331.28 g/mol): In the glovebox, [Cp*Rh(μ-Cl)(Cl)]$_2$ (50 mg, 0.081 mmol), norbornadiene (20 mg, 0.22 mmol, 2.7 equivs.), and Zn metal (100 mg, 1.53 mmol) were combined in a 20 mL scintillation vial equipped with a stir bar and dissolved in approximately 5 mL of THF and stirred for 24 h resulting in a dark orange/red solution. The reaction was filtered, washed with pentane and allowed to recrystallize at room temperature through evaporation (33 mg, 60%). **^{1}H NMR (400 MHz, C_6D_6, 298 K)**: δ_H = 3.44 (m, 4H), 2.57 (m, 2H), 1.85 (s, 15H; Cp*(CH_3)) 1.03 (app. t, 2H, J = 1.6 Hz; NBD CH_2).

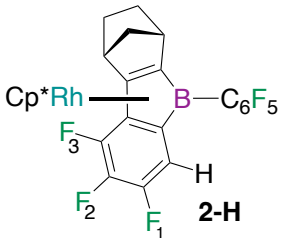

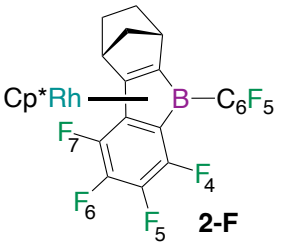

[Cp*Rh(1-boraindene-F)] (**2-F**; $C_{29}H_{23}BF_9Rh$, Mw = 656 g/mol) and **[Cp*Rh(1-boraindene-H)]** (**2-H**; $C_{29}H_{24}BF_8Rh$, Mw = 638 g/mol): In the glovebox, [Cp*Rh(NBD)] (35 mg, 0.10 mmol) and HB(C_6F_5)$_2$ (35 mg, 0.10 mmol) were combined in 2 mL toluene. The reaction was stirred for 1 h at room temperature during which the solution turned from yellow orange to dark orange. The reaction mixture was then evaporated to dryness *in-vacuo*. 1 mL of pentane was added to dissolve the solid material and the sample was placed on a shelf at 25 °C overnight, depositing orange crystals of **2-H** and **2-F** as a 1:1 mixture (17 mg, 26%). Isolated yields ranging from 25-30% were consistently obtained (**Figure S13** shows crude versus recrystallized). **^{1}H NMR (400 MHz, C_6D_6, 298 K):** δ_H = 6.88 (ddd, $^3J_{F,F}$ = 11.2 Hz, $^4J_{F,F}$ = 7.0 Hz, $^5J_{F,F}$ = 1.5 Hz; **2-H** ArH), 3.09 (1H, **2-H** NBD(CH)), 3.03 (1H, **2-F** NBD(CH)), 2.84 (1H, **2-H** NBD(CH)), 2.78 (1H, **2-F** NBD(CH)), 1.25 (15H; **2-F** Cp*(CH_3)), 1.21 (15H; **2-H** Cp*(CH_3)), 1.59-1.54 (4H, **2-H** + **2-F** NBD(CH)), 1.33 (2H, **2-H** + **2-F** NBD(CH) by ^{1}H-^{1}H COSY), 1.14-1.10 (4H, **2-H** + **2-F** NBD(CH)), 0.92 (2H, **2-H** + **2-F** NBD(CH) by ^{1}H-^{1}H COSY). **^{19}F{^{1}H} NMR (564.8 MHz, C_6D_6, 298 K):** δ_F = -127.3 (m, 2F; **2-H** *o*-B(C_6F_5)), -127.4 (m, 2F; **2-F** *o*-B(C_6F_5)), -131.5 (m, 1F; **2-F**, **F$_4$**), -136.2 (dd, $^3J_{F,F}$ = 17.8 Hz, $^4J_{F,F}$ = 3.3 Hz, 1F; **2-H**, **F$_1$**), -145.9 (dd, $^3J_{F,F}$ = 16.5 Hz, $^3J_{F,F}$ = 3.5 Hz, 1F; **2-H**, **F$_3$**), -151.5 (dd, $J_{F,F}$ = 23.7 Hz, $J_{F,F}$ = 16.2 Hz, $J_{F,F}$ = 2.2 Hz, 1F; **2-F**, **F$_7$**), -156.8 (app. t, $J_{F,F}$ = 20.5 Hz, 1F; **2-F** *p*-B(C_6F_5)), -157.1 (app. t, $J_{F,F}$ = 20.7 Hz, 1F; **2-H** *p*-B(C_6F_5)), -160.0 (app. t, $J_{F,F}$ = 16.7 Hz, 1F; **2-F**, **F$_6$**), -163.4 (app. t, $J_{F,F}$ = 16.5

Hz, 1F; **2-H**, **F$_2$**), -163.7 (m, 2F; **2-H** *m*-B(C$_6$F$_5$)), -164.2 (m, 2F; **2-F** *m*-B(C$_6$F$_5$)), -164.9 (app. t, $J_{F,F}$ = 17.6 Hz, 1F; **2-F**, **F$_5$**). **^{11}B{^{1}H} NMR (128.3 MHz, C$_6$D$_6$, 298 K):** δ_B = 4.6 ($\Delta_{1/2}$ = 250 Hz). **^{13}C{^{1}H} NMR (125.8 MHz, C$_6$D$_6$, 298 K, select signals):** δ_C = 148.1 (dm, $^1J_{F,C}$ = 238 Hz, *o*-B(C$_6$F$_5$)), 138.8 (dm, $^1J_{F,C}$ = 269 Hz *p*-B(C$_6$F$_5$)), 138.0 (dm $^1J_{F,C}$ = 256 Hz, *m*-B(C$_6$F$_5$), n.o. (*i*-B(C$_6$F$_5$)), 112.8, 108.1, 107.6, 95.9 ($^1J_{Rh,C}$ = 6.6 Hz; Cp*(C)), 95.3 ($^1J_{Rh,C}$ = 6.3 Hz; Cp*(C)), 47.9, 47.2, 46.9, 39.4, 39.2, 39.1, 38.8, 37.0, 36.69, 27.4, 27.3, 26.6, 26.4, 8.66 (Cp*(CH$_3$), 8.45 (Cp*(CH$_3$). **HRMS (APCI)**: *m*/*z* [M]$^+$ calcd. for **2-H**: [C$_{29}$H$_{24}$BF$_8$Rh]$^+$: 638.090; found: 638.089, *m*/*z* [M]$^+$ calcd. for **2-F** [C$_{29}$H$_{23}$BF$_9$Rh]$^+$: 656.080; found: 656.079.

Alternative Reaction Conditions:

- **Reaction at -78 °C.** In a glovebox, [Cp*Rh(NBD)] (18 mg, 0.05 mmol) and HB(C$_6$F$_5$)$_2$ (19 mg, 0.05 mmol) were independently weighed and dissolved in ~1 mL of toluene and cooled to –78 °C in a cold well. Both reagents were mixed at –78 °C and stirred for 30 minutes, then allowed to warm to room temperature. The solution was transferred to a J. Young NMR tube and analyzed by ^{19}F{^{1}H} NMR spectroscopy, which indicated exclusive formation of **2-F** in 24% yield by ^{19}F{^{1}H} NMR spectroscopy using fluorobenzene as an internal standard.

- **Reaction using [D(BC$_6$F$_5$)$_2$]$_2$:** In a glovebox, [Cp*Rh(NBD)] (6 mg, 0.018 mmol) and DB(C$_6$F$_5$)$_2$ (6 mg, 0.017 mmol) were dissolved in *3* mL of toluene at 25 °C. The reaction mixture was stirred for 30 minutes, transferred to a J. Young NMR tube, and analyzed by ^{19}F{^{1}H} NMR spectroscopy, which indicated formation of **2-F**:**2-H** in a 3:1 ratio in 28% and 8% yield by ^{19}F{^{1}H} NMR spectroscopy using fluorobenzene as an internal standard.

- **Reaction with B(C$_6$F$_5$)$_3$ additive:** In a glovebox, [Cp*Rh(NBD)] (17 mg, 0.05 mmol) was added to an 3 mL toluene solution at 25 °C containing a 1:1 mixture of B(C$_6$F$_5$)$_3$ (9 mg, 0.03 mmol) and HB(C$_6$F$_5$)$_2$ (9 mg, 0.02 mmol). The reaction mixture was stirred for 30 minutes, transferred to a J. Young NMR tube, and analyzed by ^{19}F{^{1}H} NMR spectroscopy, which

indicated exclusive formation of **2-F** in 28% yield by $^{19}F\{^{1}H\}$ NMR spectroscopy using fluorobenzene as an internal standard.

***exo*-Bicyclo[2.2.1]hept-2-yldi(pentafluorophenyl)borane** (**3**; $C_{19}H_9BF_{10}$, Mw = 438.1 g/mol): In the glovebox, $HB(C_6F_5)_2$ (37.5 mg, 0.11 mmol) and norbornadiene (10 mg, 0.11 mmol) were combined in a 20 mL scintillation vial equipped with a stir bar and dissolved in approximately 5 mL of toluene and stirred for 5 mins resulting in a clear colorless solution. The reaction was filtered and washed with cold pentane, giving a colorless oily solid (33 mg, 69%). **^{1}H NMR (400 MHz, C_6D_6, 298 K)**: δ_H = 6.15 (m, 1H), 5.96 (m, 1H), 2.95 (s, 1H), 2.78 (s, 1H), 1.83 (m, 1H), 1.69 (m, 1H), 1.31 (m, 1H), 1.20 (m, 1H), 0.78 (m, 1H). **$^{19}F\{^{1}H\}$ NMR (564.8 MHz, C_6D_6, 298 K):** δ_F = -129.9 (m, 2F, *o*-C_6F_5), -148.6 (t, $J_{F,F}$ = 20.1 Hz, 1F, *p*-C_6F_5), -160.9 (m, 4F, *m*-C_6F_5). **$^{11}B\{^{1}H\}$ NMR (128.3 MHz, C_6D_6, 298 K):** δ_B = 73.6 ($\Delta_{1/2}$ = 800 Hz). **$^{13}C\{^{1}H\}$ NMR (125.8 MHz, C_6D_6, 298 K):** δ_C = 146.3 (dm, $^{1}J_{F,C}$ = 238 Hz, *o*-B(C_6F_5)), 143.1 (dm, $^{1}J_{F,C}$ = 269 Hz *p*-B(C_6F_5)), 137.98, 137.7 (dm $^{1}J_{F,C}$ = 256 Hz, *m*-B(C_6F_5), n.o. (*i*-B(C_6F_5)), 135.8, 47.7, 45.4, 43.0, 41.9 (br), 28.6. *N.B.* A formal *exo*-addition product is consistent with the known stereochemistry for additions of boranes to bicyclic olefins.[3]

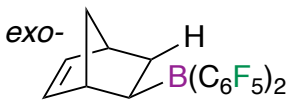

Attempted cyclization using 3. In a J. Young NMR tube, complex **3** (10 mg, 0.0068 mmol) was combined with either 10 or 100 mol% of [Cp*Rh(NBD)] (relative to **3**). The mixture was dissolved in 500 μL of toluene-d_8 and heated at 40 °C for 15 h. No conversion of **3** was observed, as determined by $^{19}F\{^{1}H\}$ NMR spectroscopy.

Attempted reactions of 2-H/F. A 1:1 mixture of complexes **2-H** and **2-F** (5-10 mg) was subjected to a range of small-molecule substrates (1-5 equivs., ~3 atm for gasses), including CO_2, CO, benzaldehyde, phenylacetylene, acetonitrile, and 2,6-dimethylphenylisonitrile, with no observable reactivity. Similarly, attempts to engage these complexes with donor ligands such as DMAP, PPh_3, PCy_3, and dppe also failed to yield any identifiable products. Reactions with oxidants such as I_2 and $PhICl_2$, intended to generate Rh(III) species, resulted in mixtures of unidentified products, suggesting non-selective or complex reactivity pathways.

3. NMR Spectroscopy:

Figure S1. 1, ^{1}H NMR, C_6D_6, 400 MHz, 298 K.

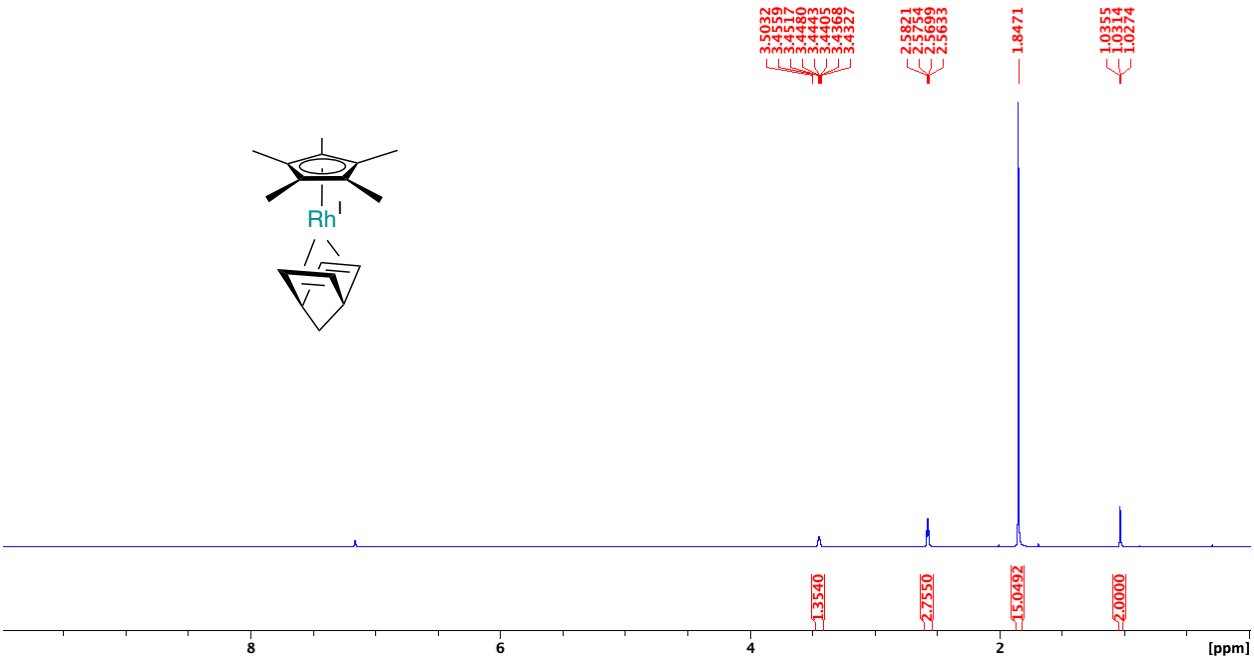

Figure S2. 2-F + **2-H**, ^{1}H NMR, C_6D_6, 400 MHz, 298 K.

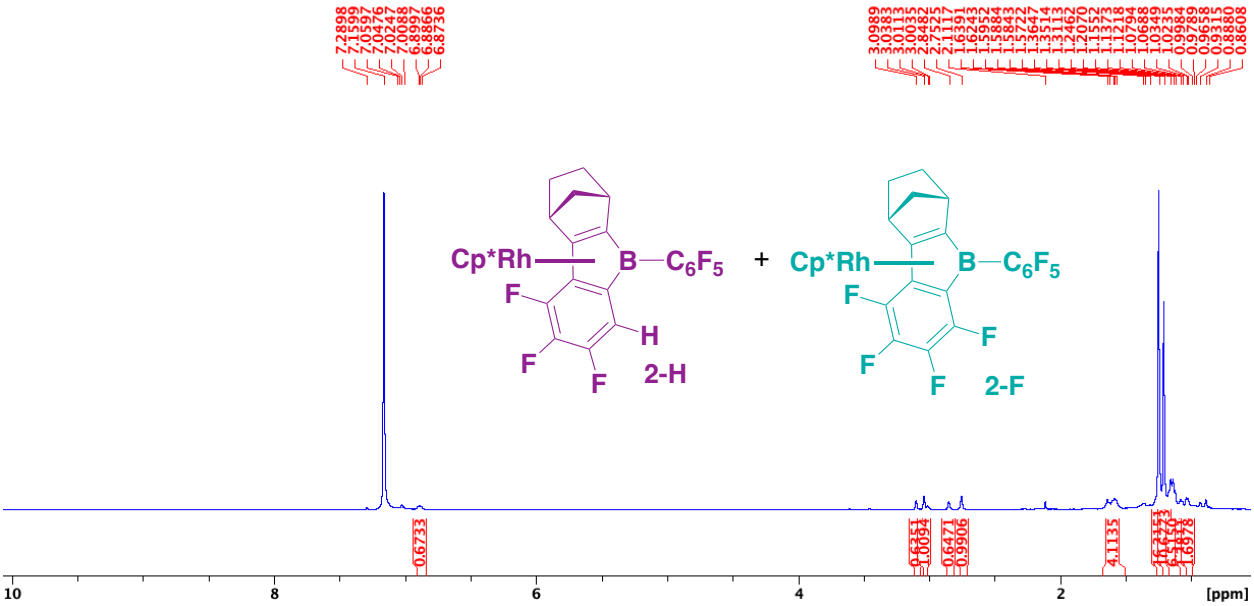

Figure S3. 2-F + **2-H**, ^{1}H NMR (expansion showing aliphatic region), C_6D_6, 400 MHz, 298 K.

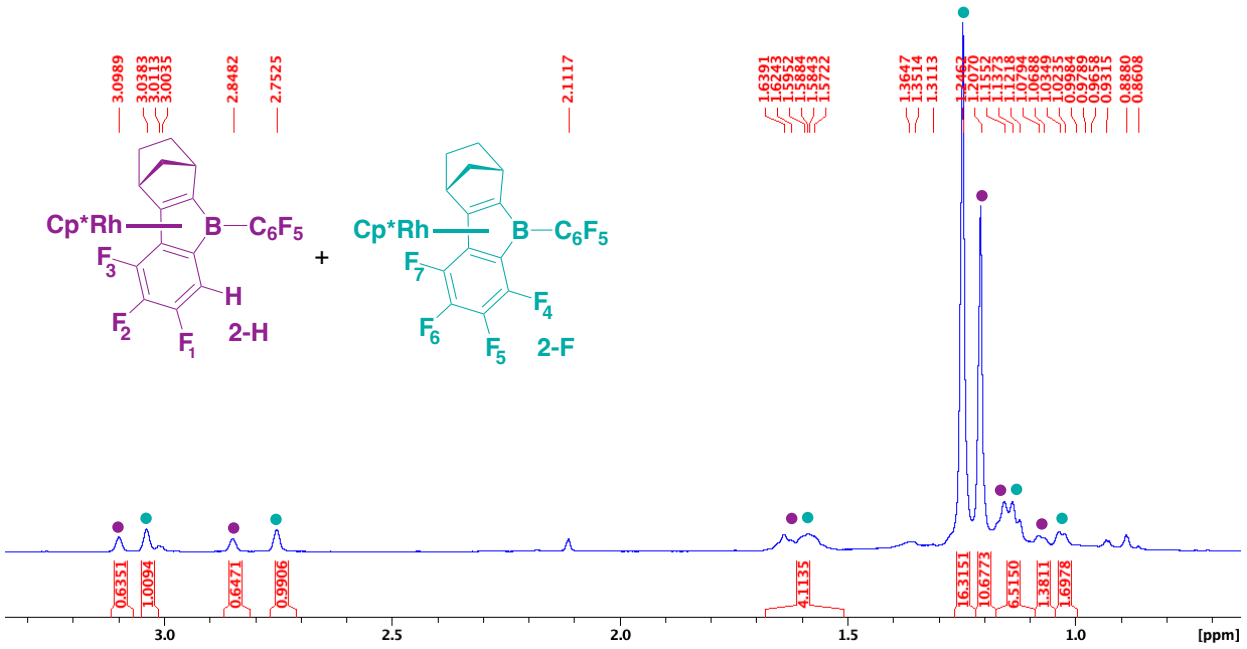

Figure S4. 2-F + **2-H**, ^{1}H NMR (expansion showing Ar-H of **2-H**), C_6D_6, 400 MHz, 298 K.

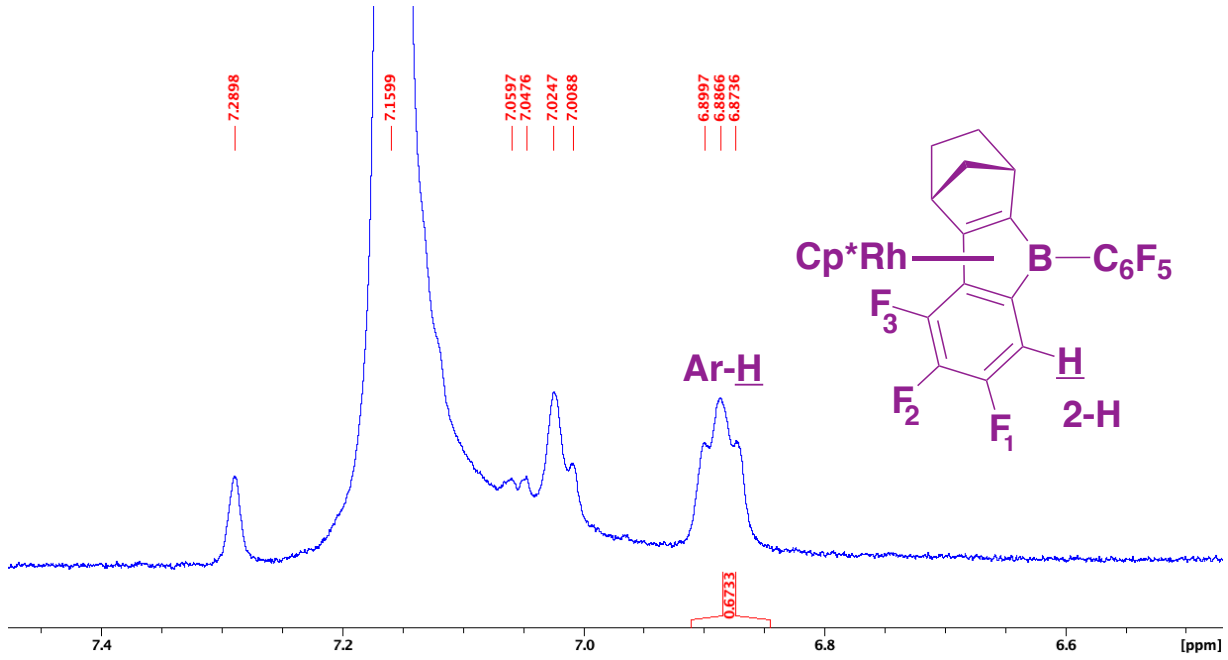

Figure S5. 2-F + **2-H**, ^{1}H-^{1}H COSY NMR, C_6D_6, 564.8 MHz, 298 K.

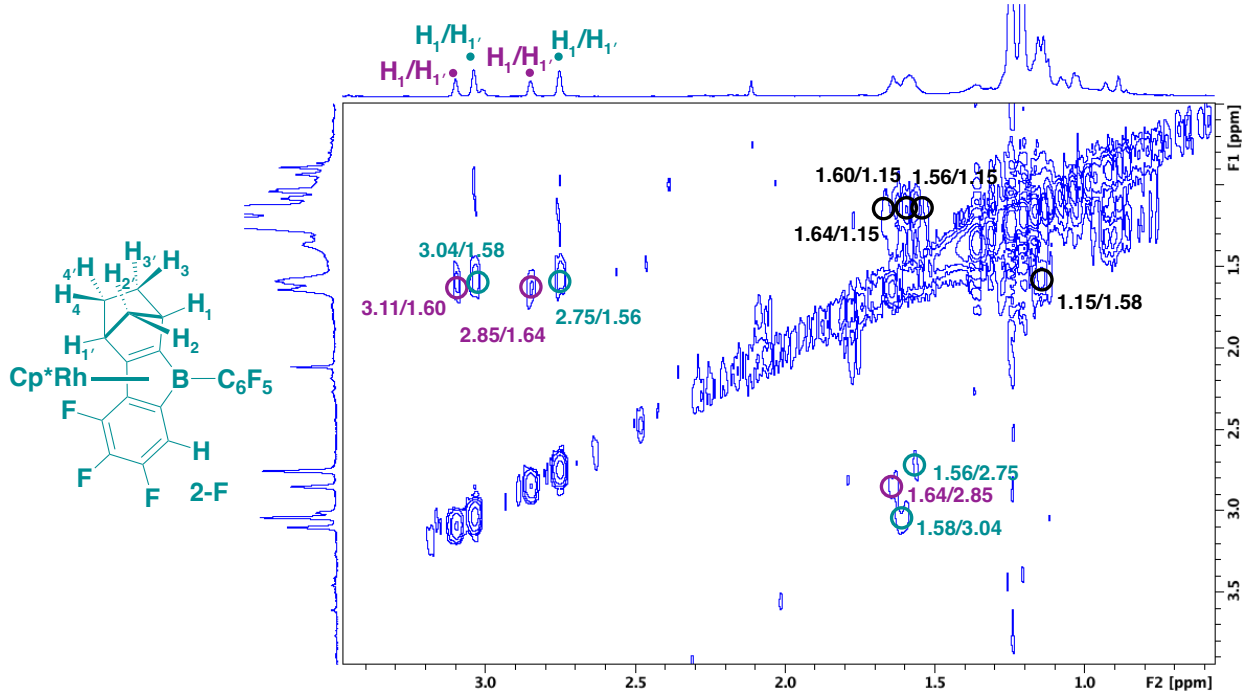

Figure S6. 2-F + **2-H**, ^{19}F NMR, C_6D_6, 564.8 MHz, 298 K.

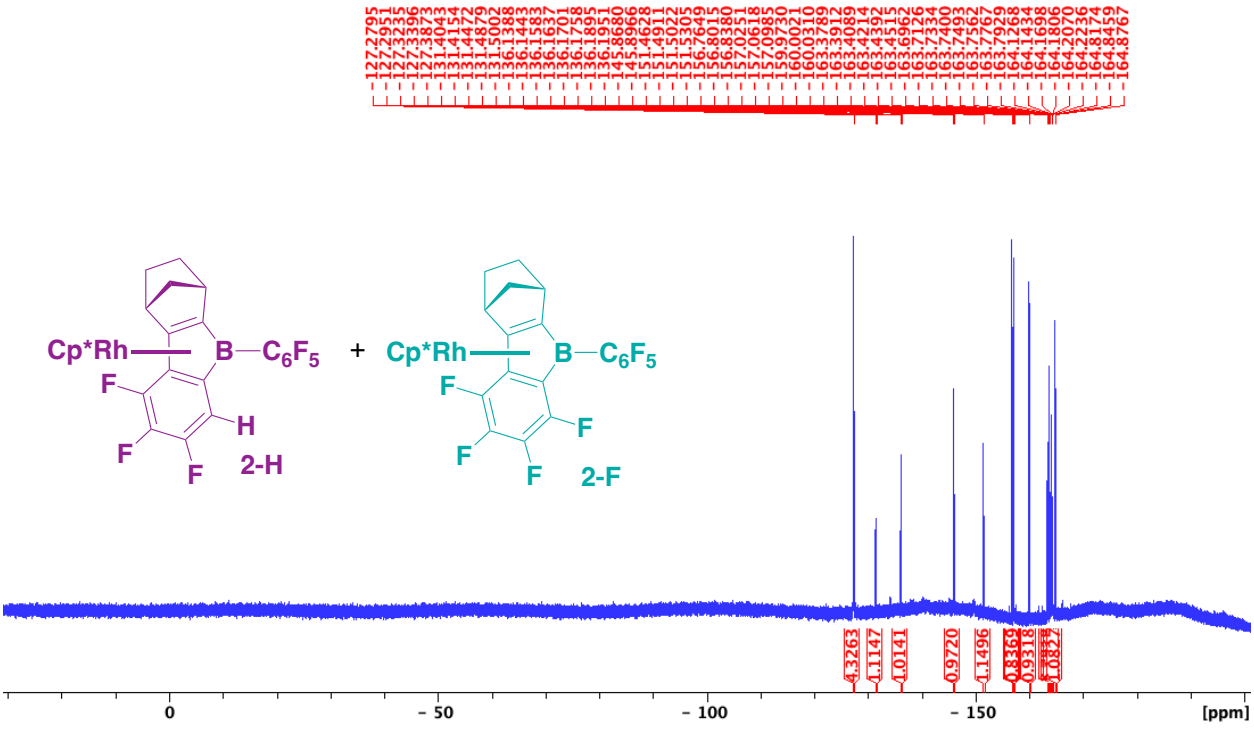

Figure S7. 2-F + **2-H**, ^{19}F NMR, C_6D_6, 564.8 MHz, 298 K.

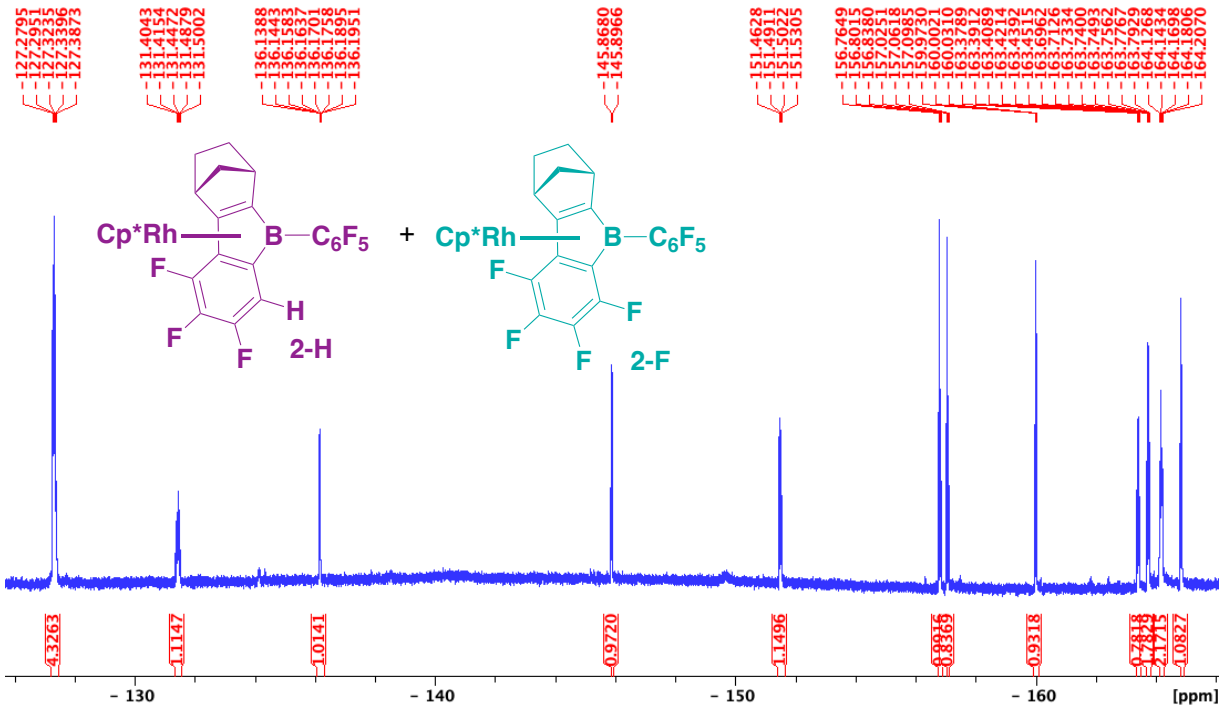

Figure S8. 2-F + **2-H**, ^{19}F NMR (expansion), C_6D_6, 564.8 MHz, 298 K.

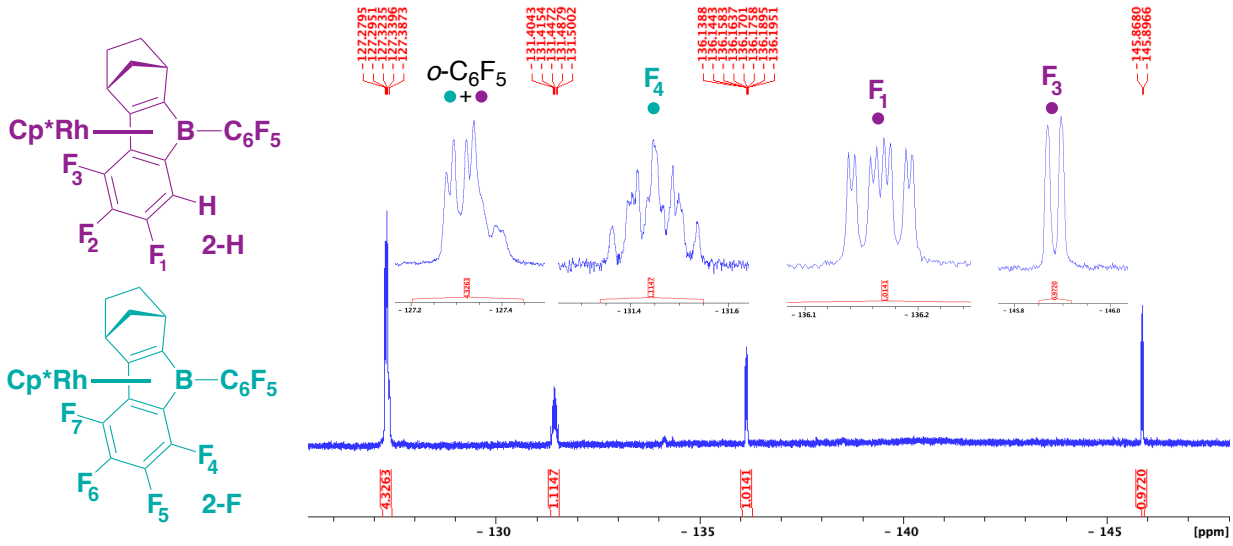

Figure S9. 2-F + 2-H, ^{19}F NMR (expansion), C_6D_6, 564.8 MHz, 298 K.

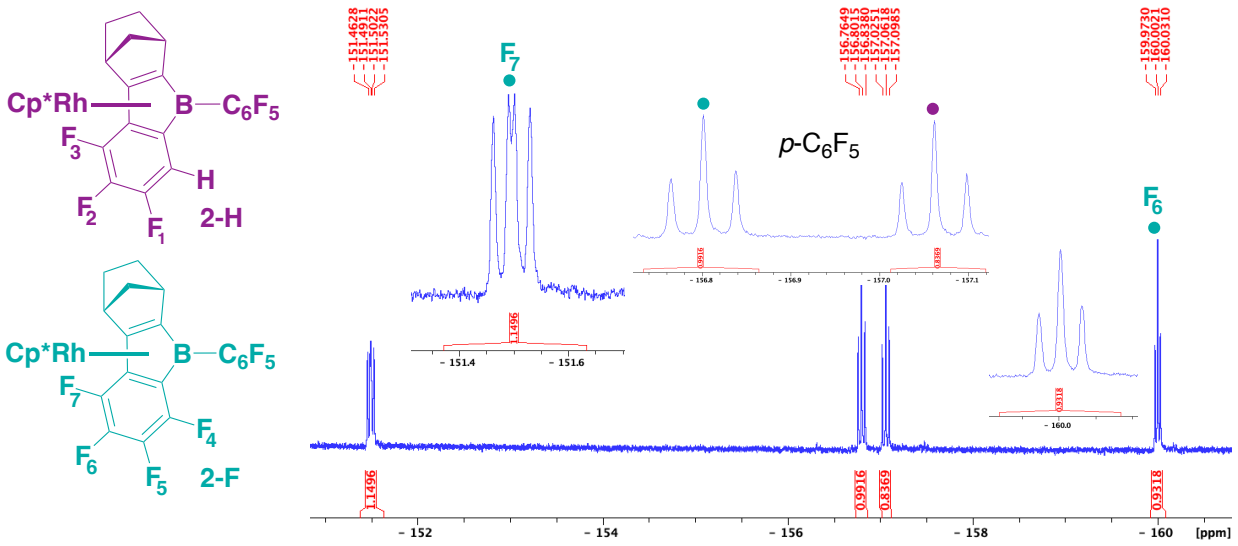

Figure S10. 2-F + 2-H, ^{19}F NMR (expansion), C_6D_6, 564.8 MHz, 298 K.

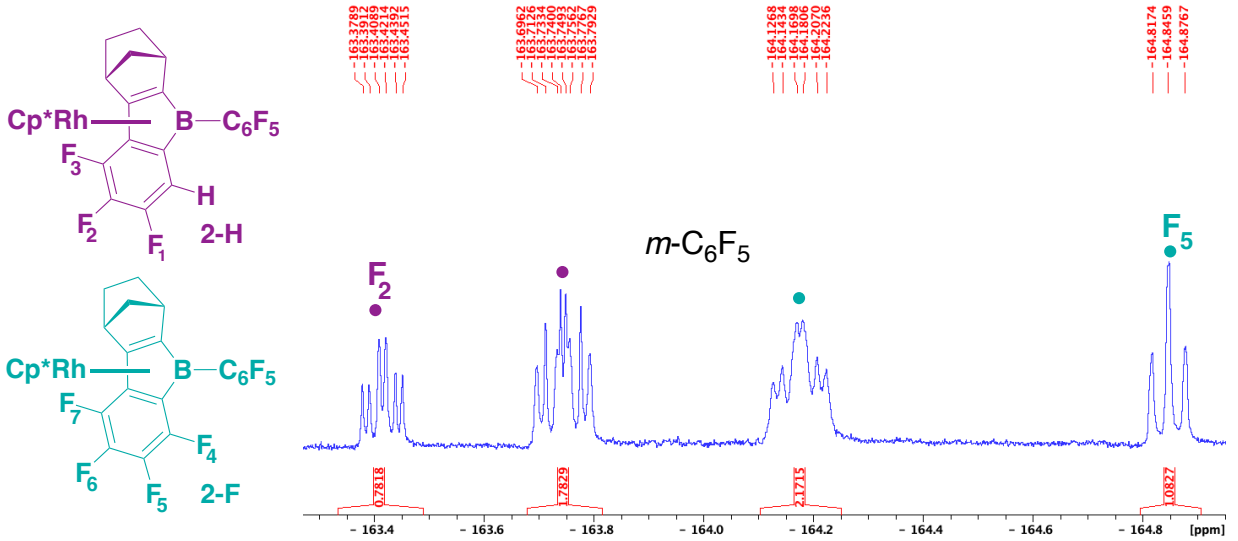

Figure S11. 2-F + 2-H, ^{19}F-^{19}F COSY NMR, C_6D_6, 564.8 MHz, 298 K.

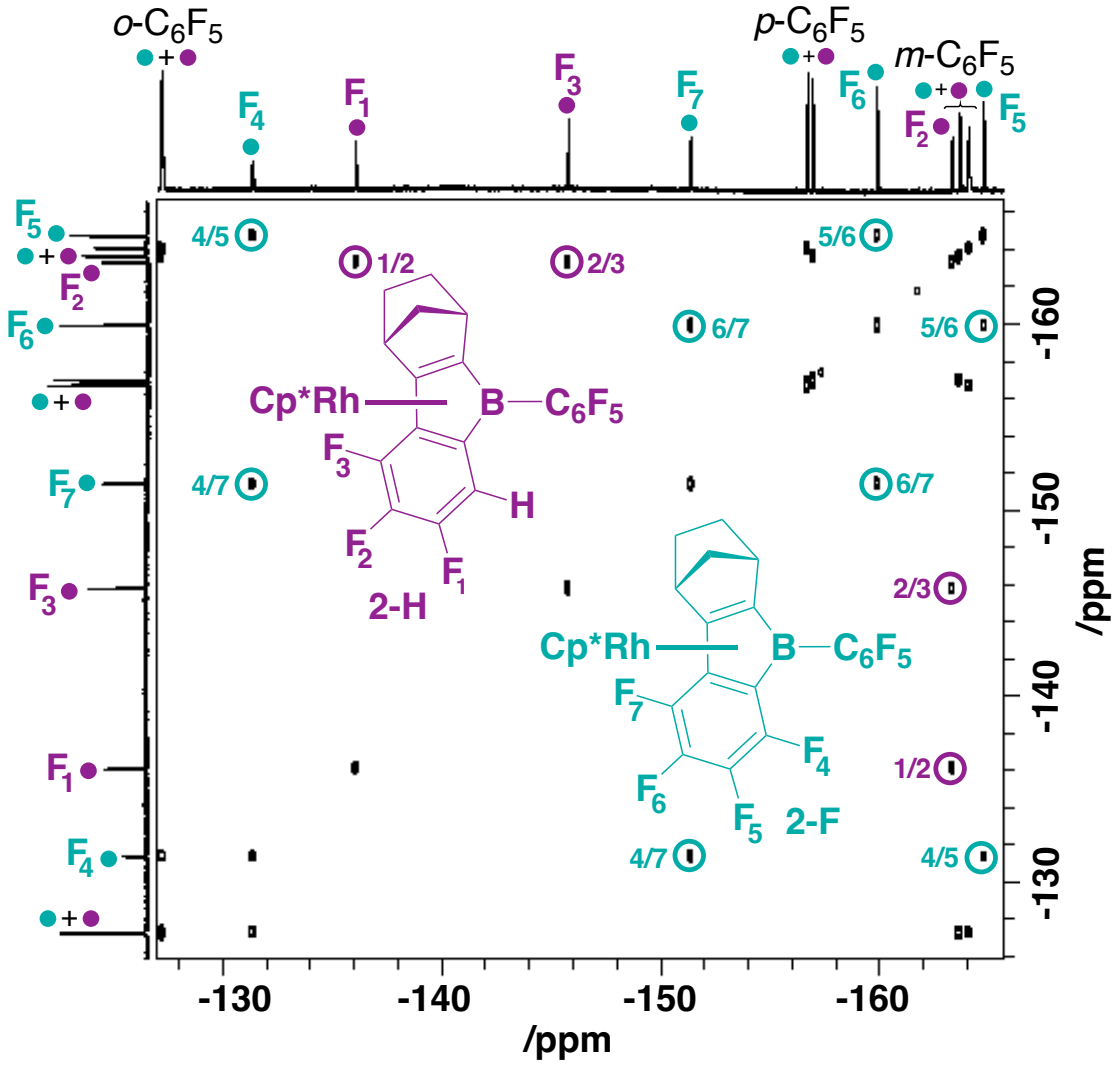

Figure S12. 2-F + 2-H (crude), stacked ^{19}F and $^{19}F\{^{1}H\}$ NMR, C_6D_6, 564.8 MHz, 298 K.

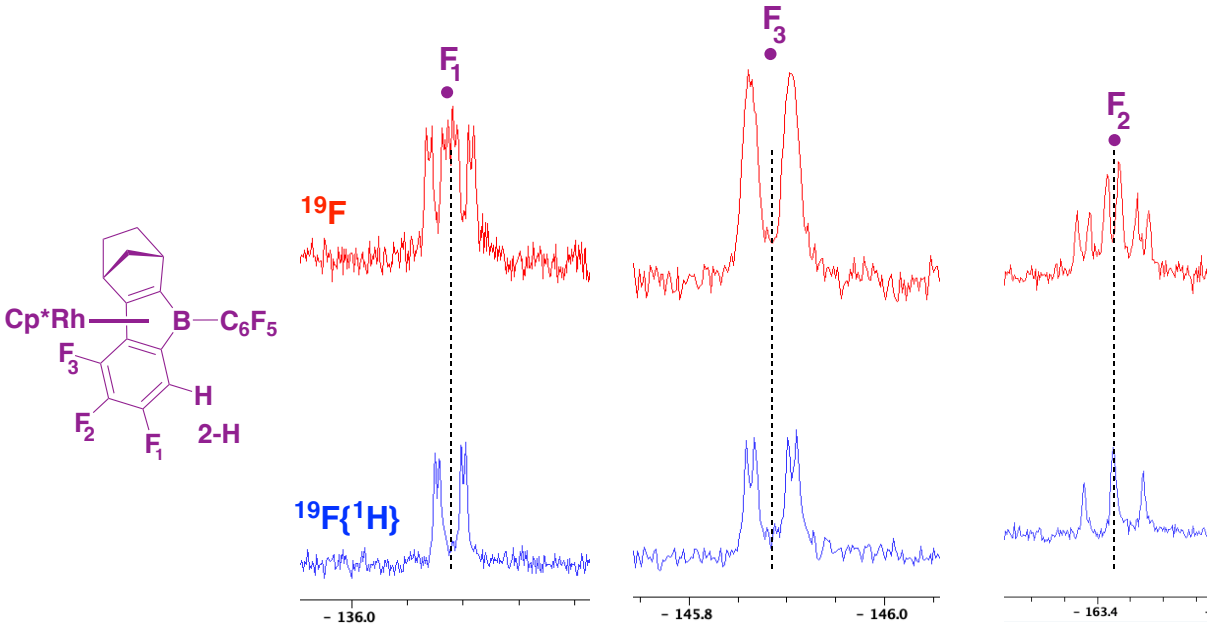

Figure S13. 2-F + 2-H (**crude** and **recrystallized**), $^{19}F\{^{1}H\}$ NMR, C_6D_6, 564.8 MHz, 298 K.

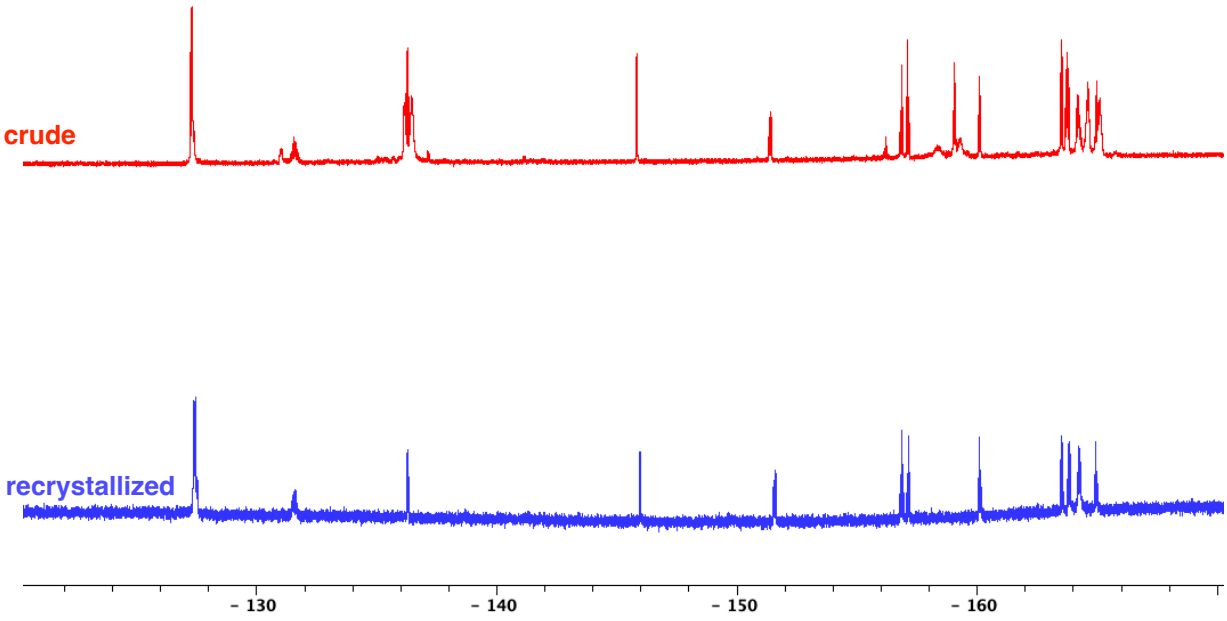

Figure S14. 2-F + **2-H**, $^{11}B\{^{1}H\}$ NMR, C_6D_6, 128.3 MHz, 298 K (*unknown impurity at δ_B = 0.12 ppm).

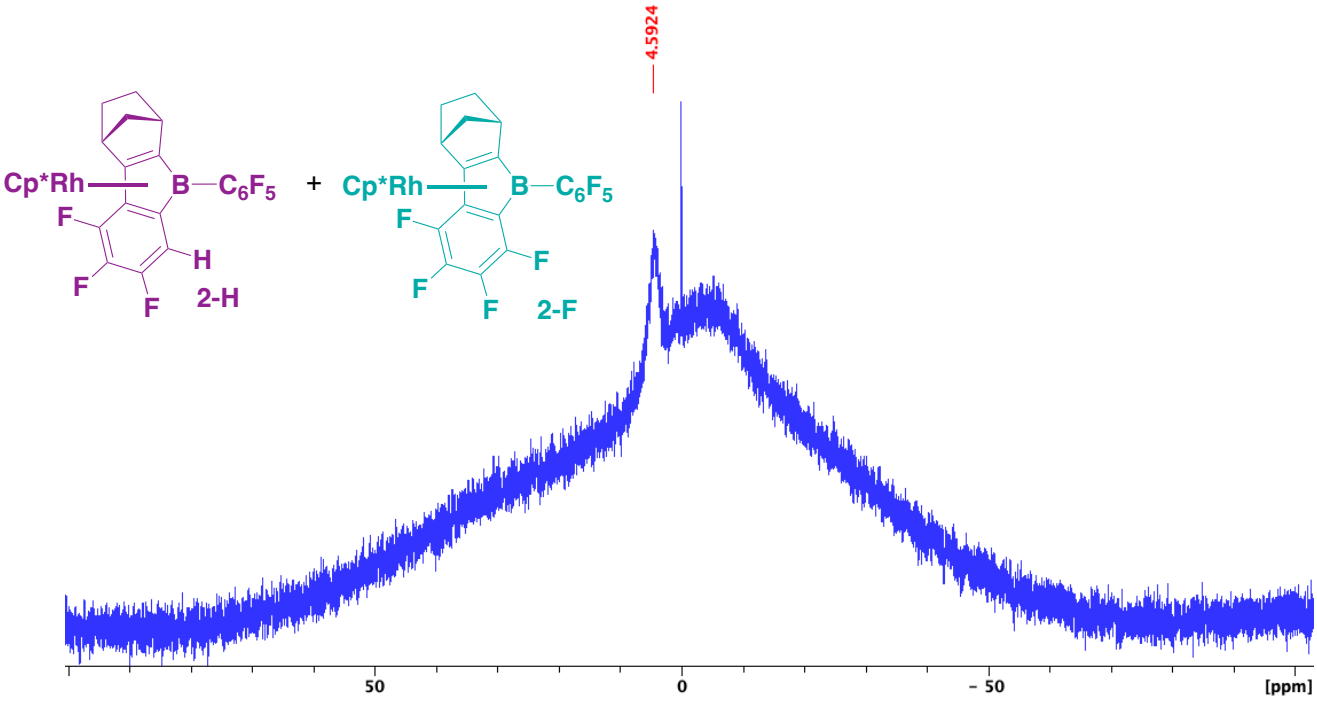

Figure S15. 2-F + **2-H**, $^{13}C\{^{1}H\}$ NMR, C_6D_6, 125.8 MHz, 298 K.

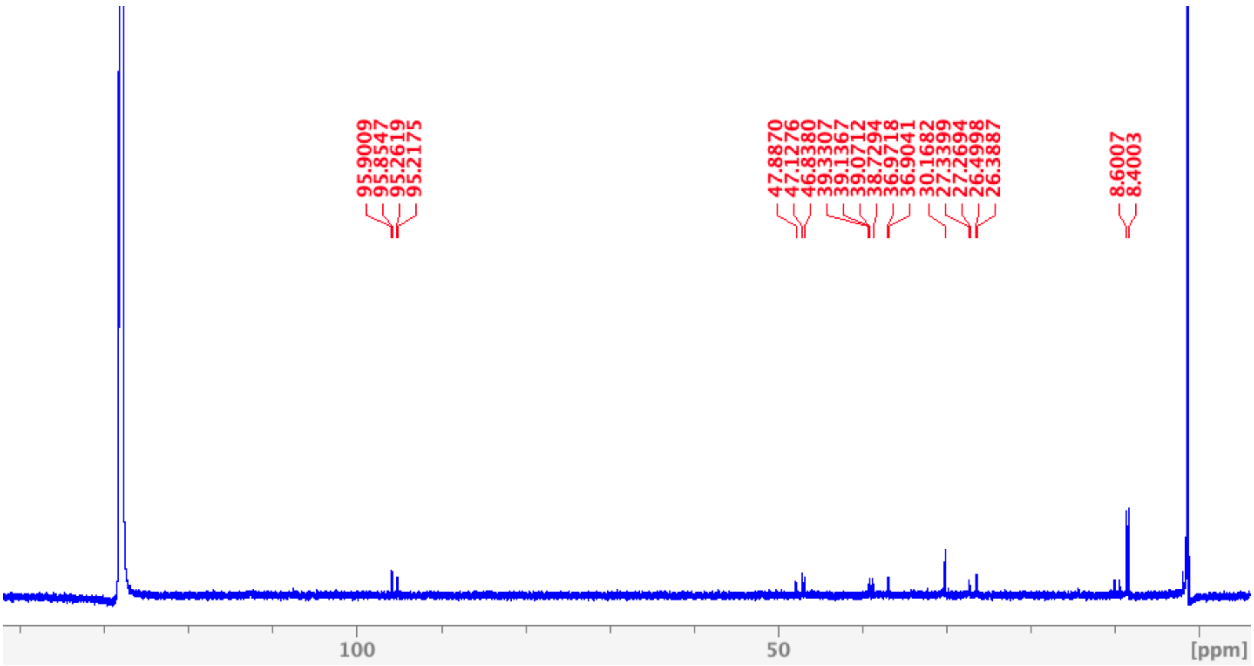

Figure S16. 2-H, $^{9}F\{^{1}H\}$ NMR, C_6D_6, 564.8 MHz, 298 K comparing the product profile at -78 °C (which gives >99% **2-F**) (**bottom**) and the room-temperature recrystallized mixture that contains a 1:1 mixture of **2-F** and **2-H** (**top**). Conclusion: reaction at -78 °C gives **2-F** exclusively.

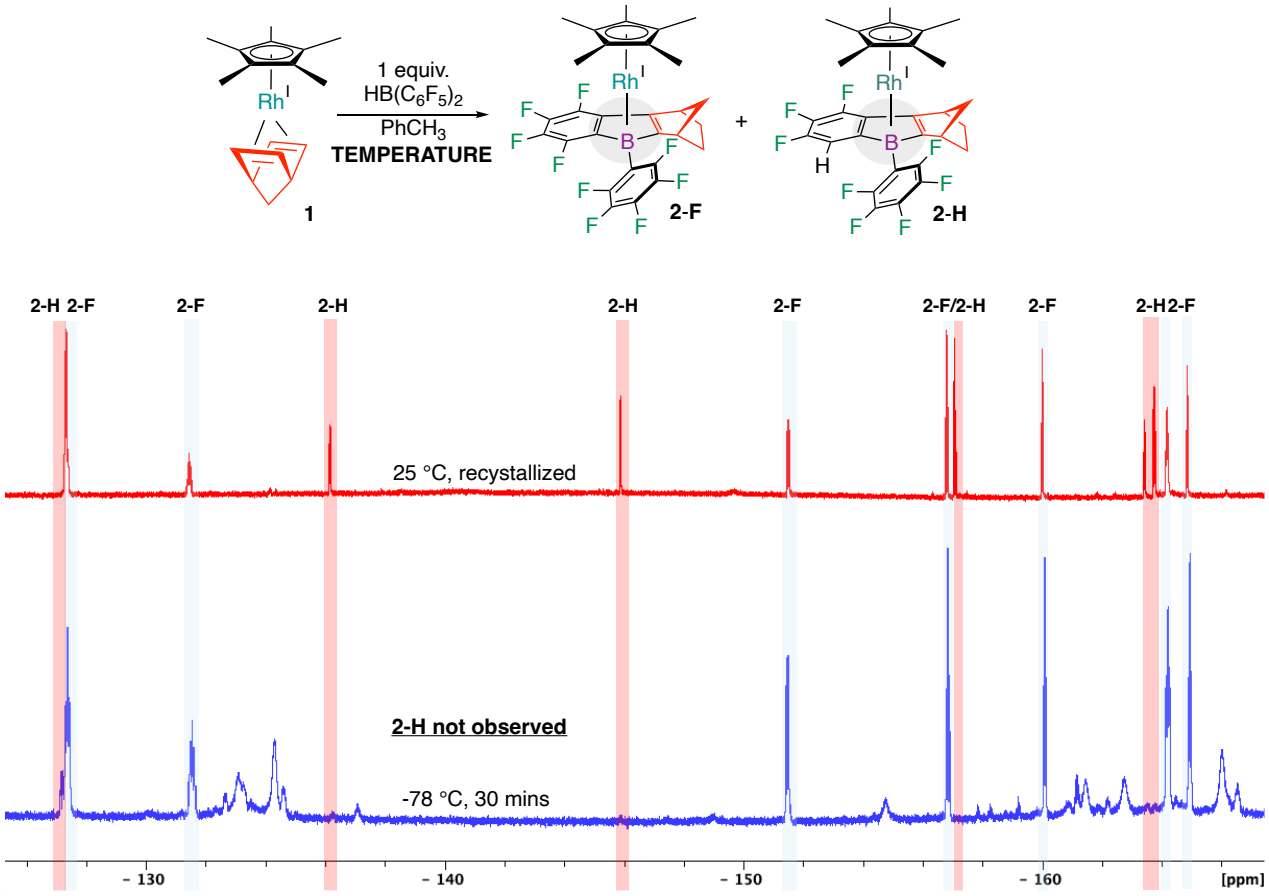

Figure S17. 2-F, $^{9}F\{^{1}H\}$ NMR, C_6D_6, 564.8 MHz, 298 K produced from reaction of [Cp*Rh(NBD)] and $HB(C_6F_5)_2$ at -78 °C (which gives >99% **2-F**).

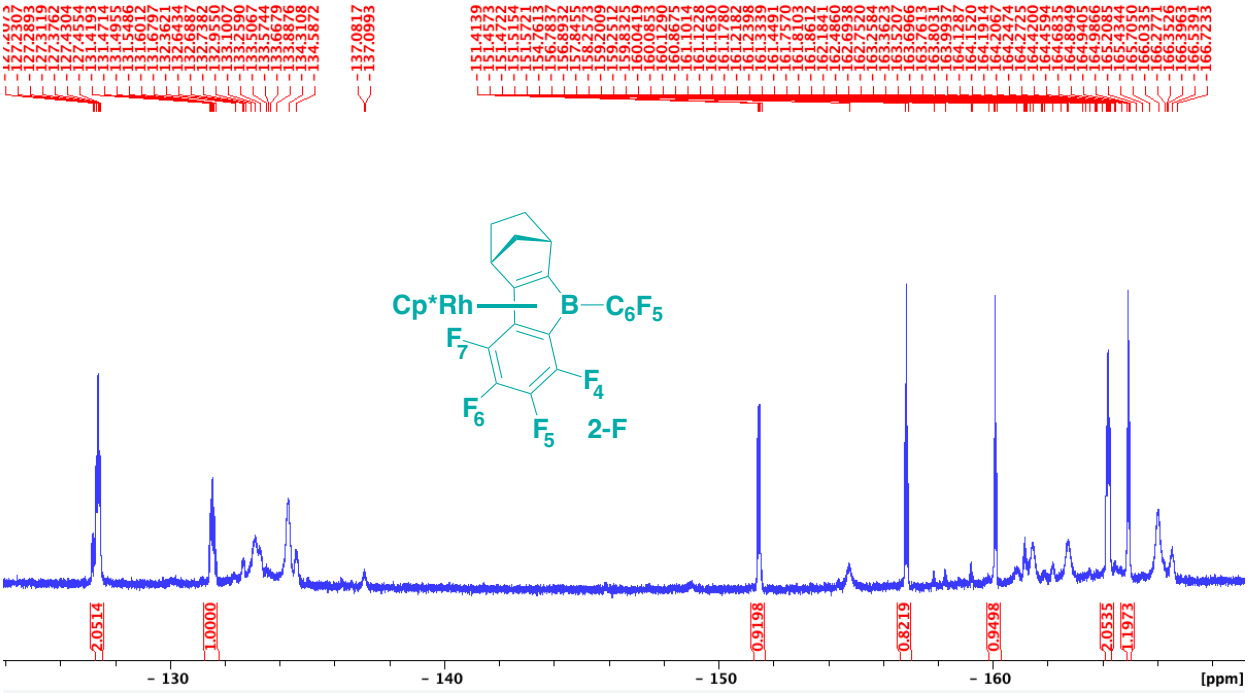

Figure S18. 2-F, ^{1}H NMR, C_6D_6, 400 MHz, 298 K produced from reaction of [Cp*Rh(NBD)] and $HB(C_6F_5)_2$ at -78 °C (which gives >99% **2-F**).

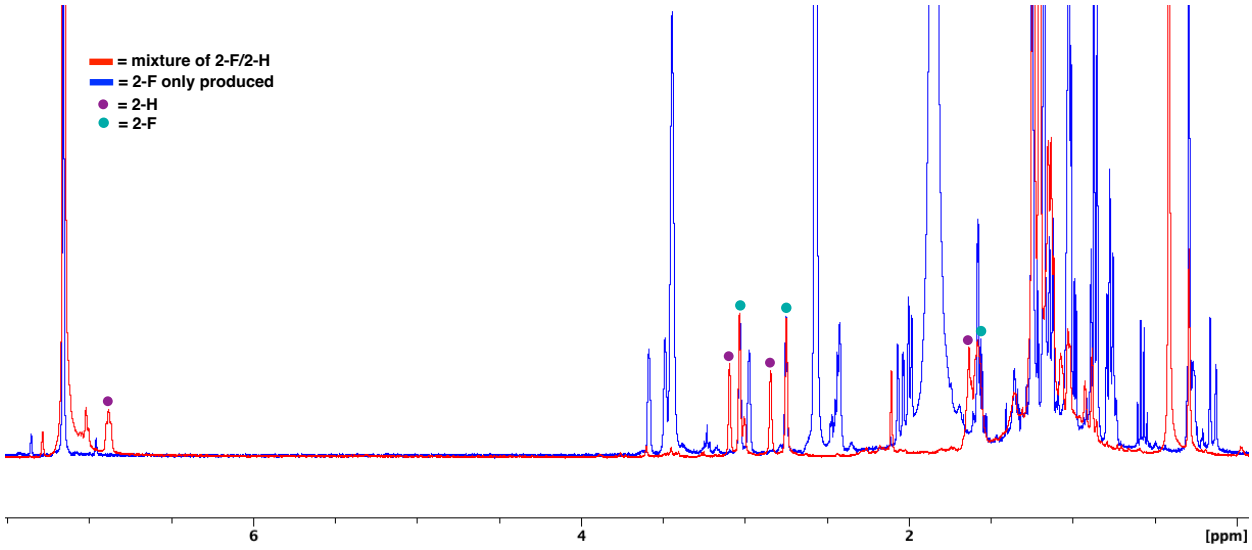

Figure S19. 3, ^{1}H NMR, C_6D_6, 400 MHz, 298 K.

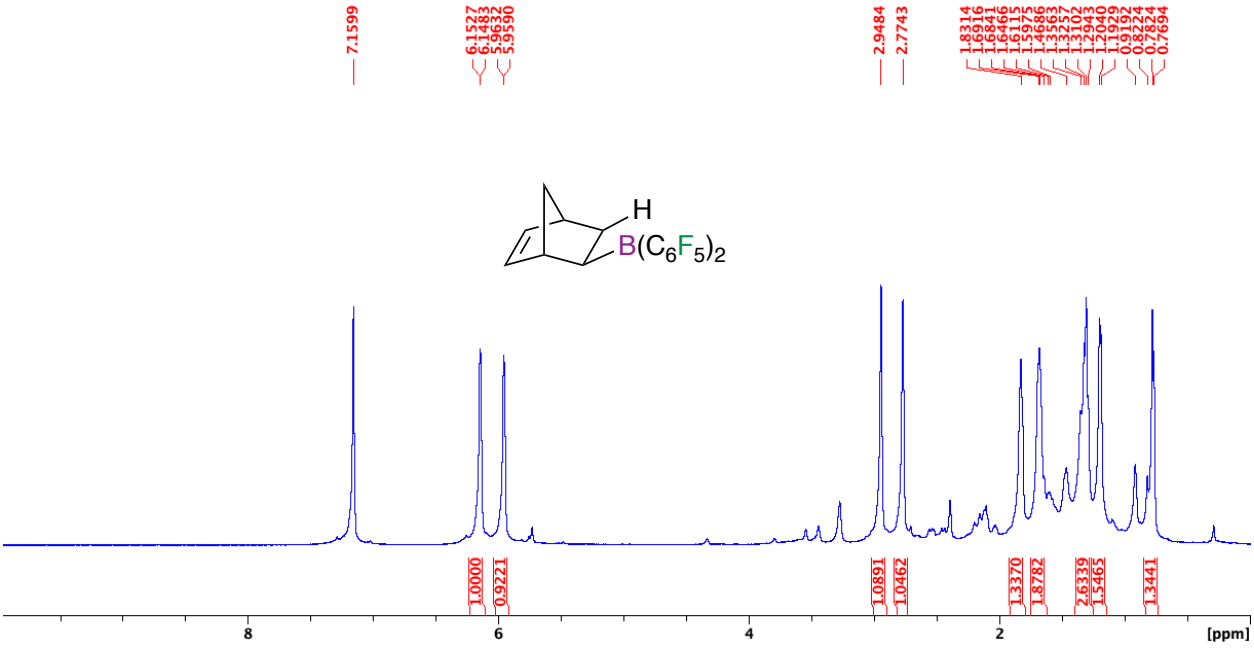

Figure S20. 3, $^{19}F\{^{1}H\}$ NMR, C_6D_6, 564.8 MHz, 298 K.

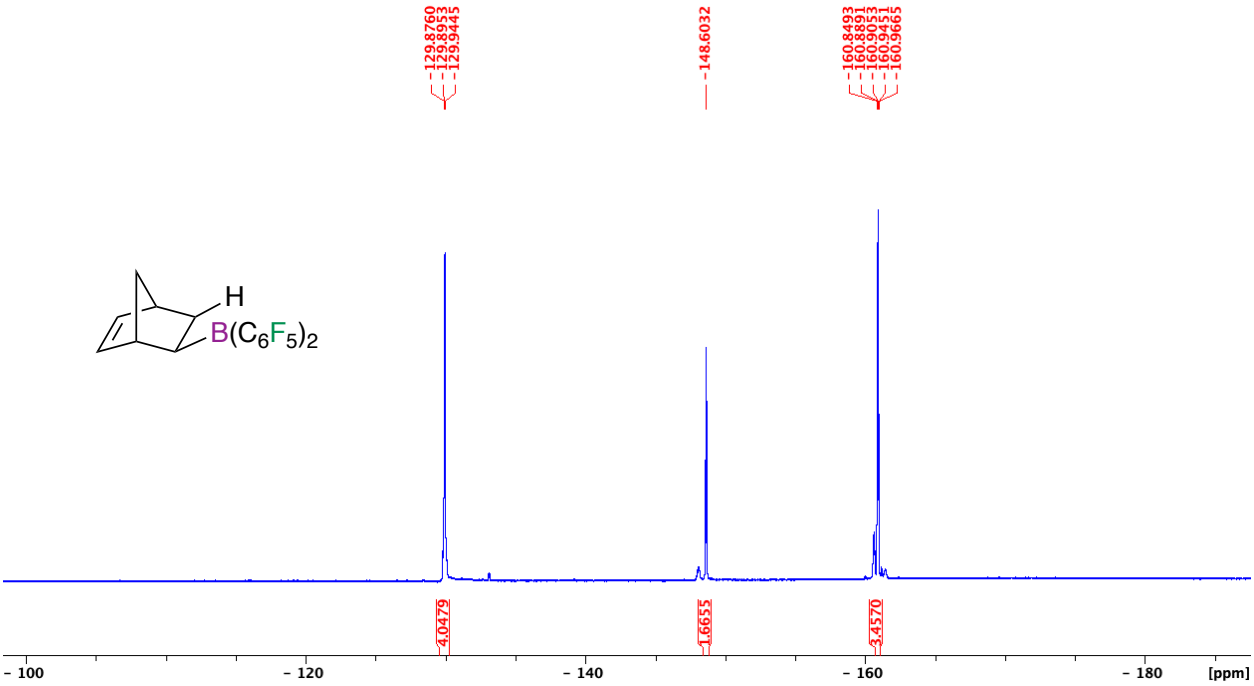

Figure S21. 3, $^{11}B\{^{1}H\}$ NMR, C_6D_6, 128.3 MHz, 298 K. Signal at $\delta_B = 0$ is borosilicate glass.

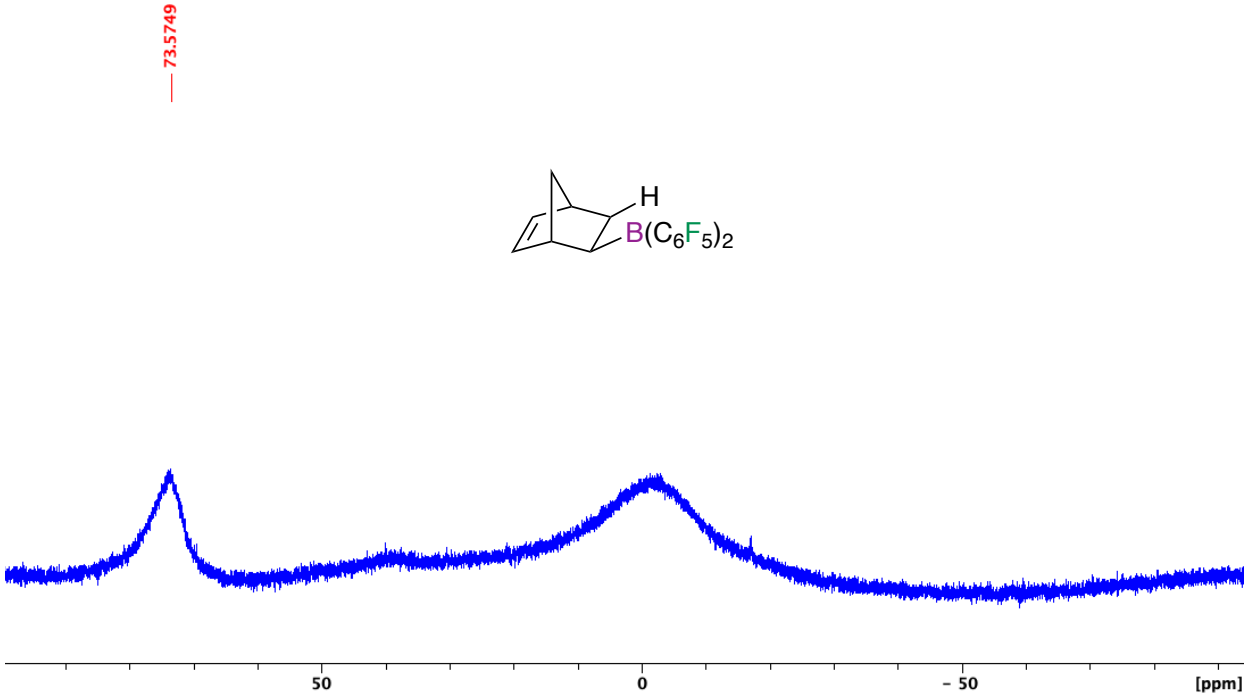

Figure 22. 3, $^{13}C\{^{1}H\}$ NMR, C_6D_6, 150.9 MHz, 298 K.

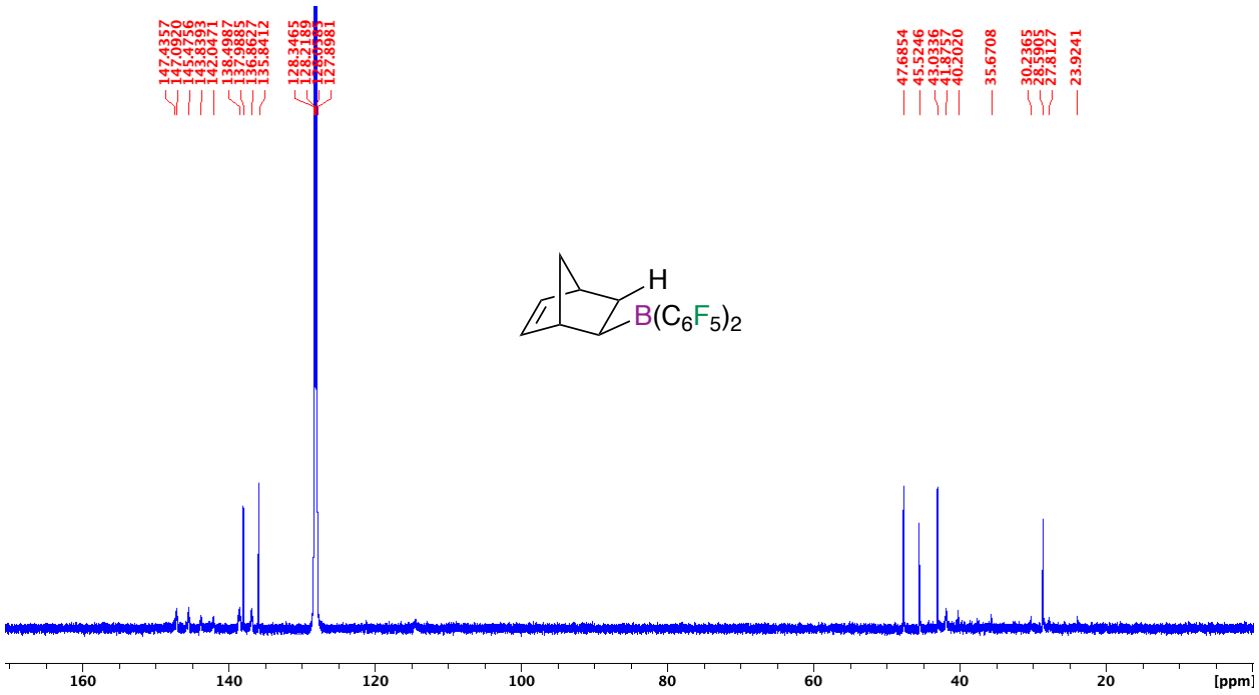

Figure S23 Reaction of *exo*-**3** with 10 mol% [Cp*Rh(NBD)], $^{19}F\{^{1}H\}$ NMR, C_6D_6, 564.8 MHz, 298 K.

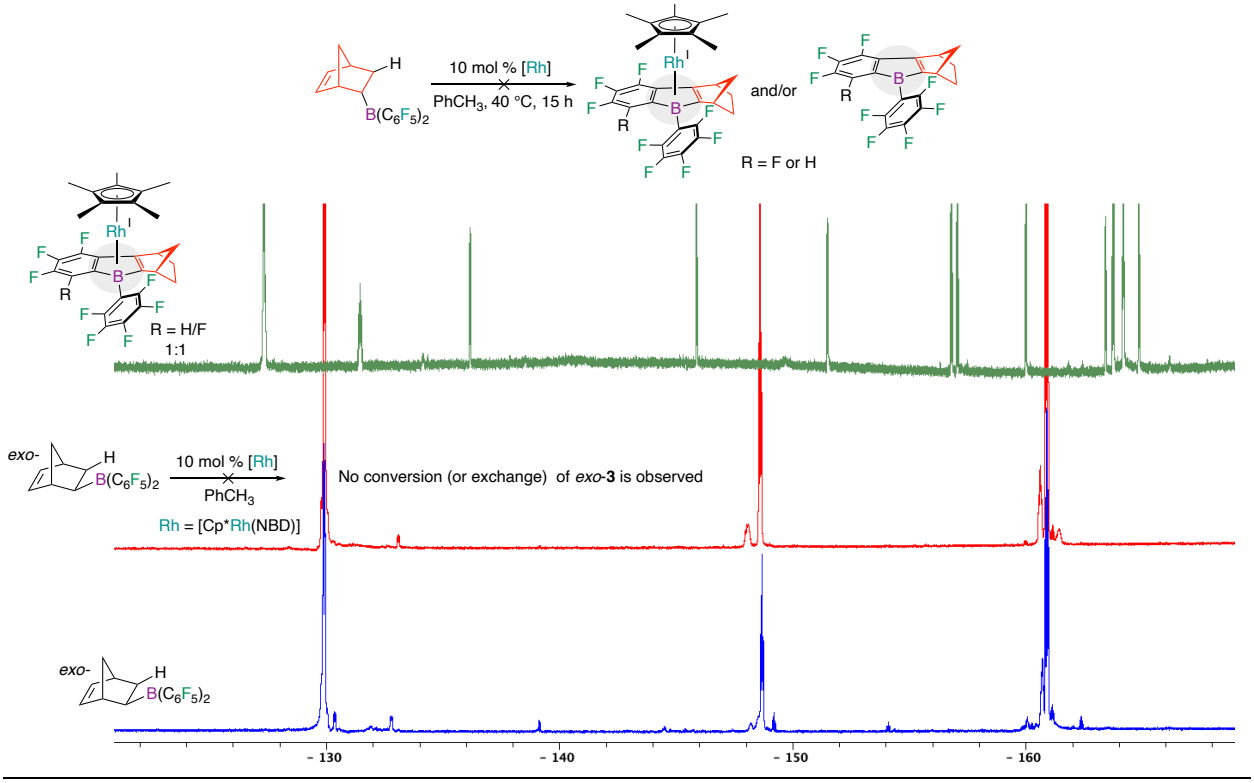

Figure S24. Stacked plot of ^{1}**H** (C_6D_6, 564.8 MHz, 298 K) (**top**) and ^{2}**H** NMR (C_6H_6, 91.7 MHz, 298 K) (**bottom**), comparing the product profile obtained from reaction of [Cp*Rh(NBD)] with $HB(C_6F_5)_2$ (^{1}**H** NMR) or $DB(C_6F_5)_2$ (^{2}**H** NMR). **Conclusion**: the ^{2}H is not localized in the ArH group, but rather in the NBD(CH) fragment.

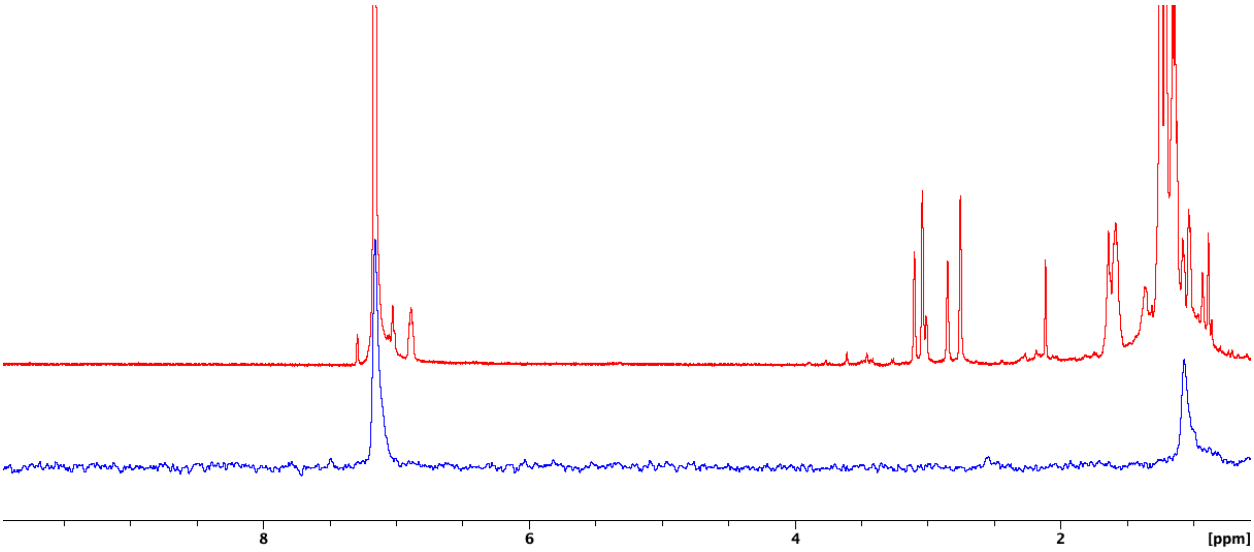

Figure S25. Stacked plot (expansion of **Figure S24**) of ^{1}**H** (C_6D_6, 564.8 MHz, 298 K) (**top**) and ^{2}**H** NMR (C_6H_6, 91.7 MHz, 298 K) (**bottom**), comparing the product profile obtained from reaction of [Cp*Rh(NBD)] with $HB(C_6F_5)_2$ (^{1}**H** NMR) or $DB(C_6F_5)_2$ (^{2}**H** NMR). **Conclusion**: the ^{2}H is not localized in the ArH group, but rather in the NBD(CH) fragment.

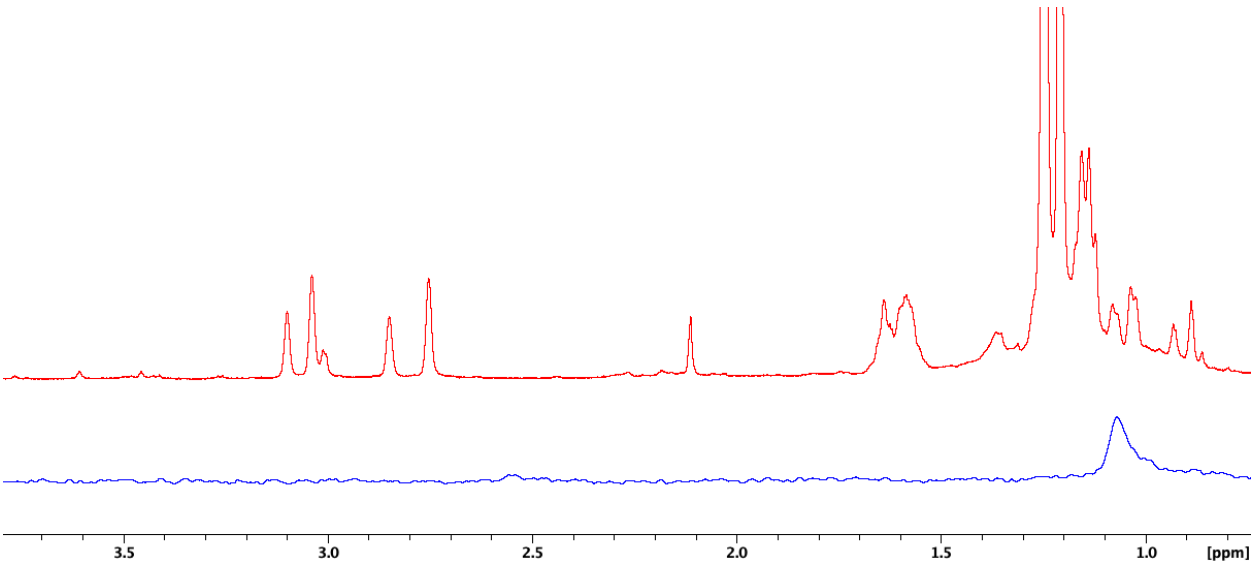

Figure S26. $^{19}F\{^{1}H\}$ NMR, C_6D_6, 564.8 MHz, 298 K comparing the product profile where 1 equiv. $B(C_6F_5)_3$ was added at 25 °C (which gives >99% **2-F**) (**bottom**) and the room-temperature recrystallized mixture that contains a 1:1 mixture of **2-F** and **2-H** (**top**). Conclusion: addition of 1 equiv. $B(C_6F_5)_3$ supresses **2-H** formation.

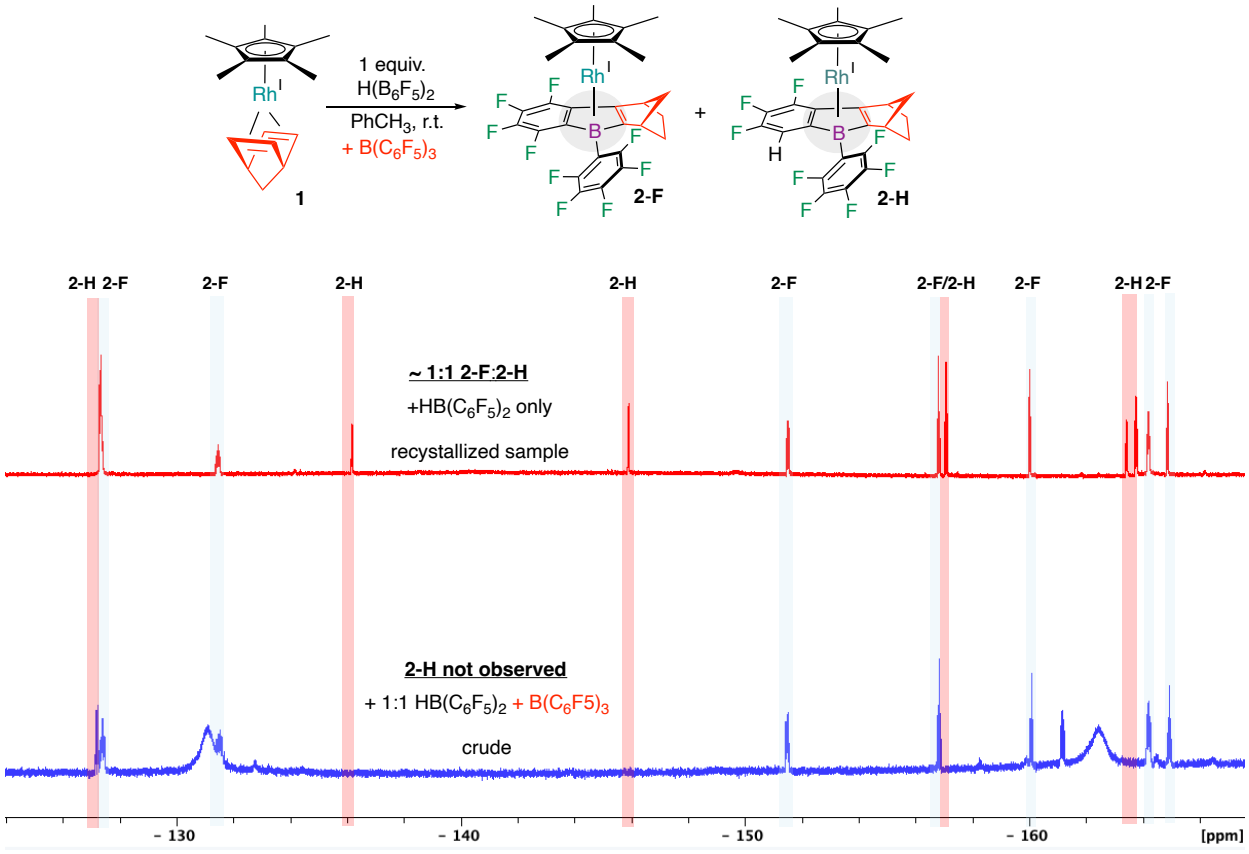

4. Mass Spectrometry:

Figure S27. 2-F + **2-H**, Mass Spectrometry - APCI (expanded) for **2-H** *m/z* = 638.0890 and **2-F** *m/z* = 656.0795.

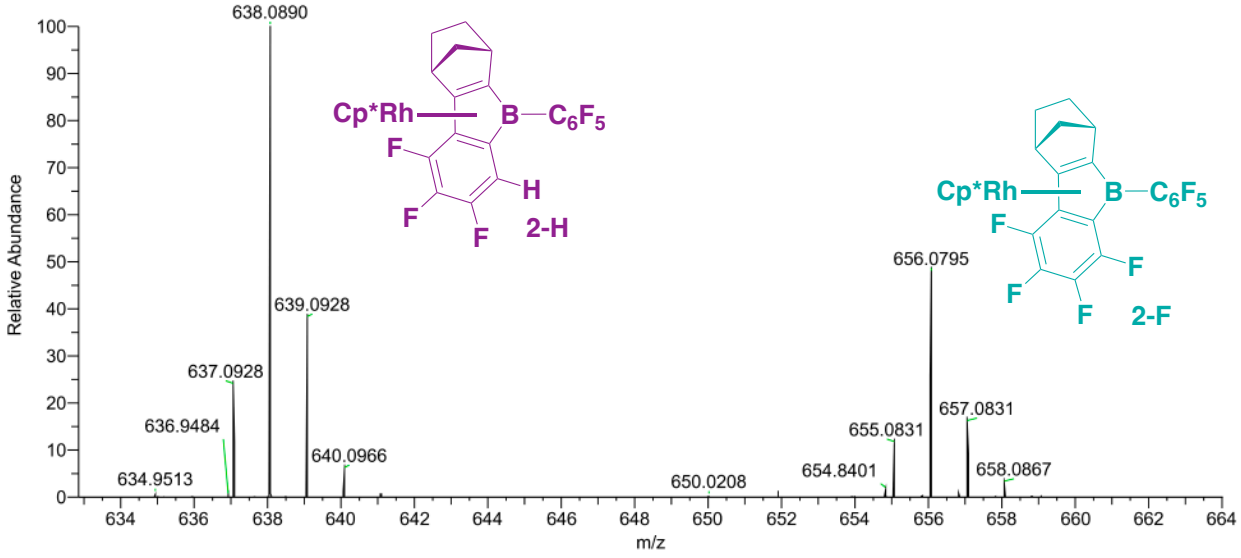

Figure S28. 2-F + **2-H**, Mass Spectrometry - APCI top (experimental), bottom (theoretical). calcd. for **2-H**: $[C_{29}H_{24}{}^{11}BF_8{}^{103}Rh]^+$: 638.0893; found: 638.0889, *m/z* $[M]^+$ calcd. for **2-F** $[C_{29}H_{23}{}^{11}BF_9{}^{103}Rh]^+$: 656.0799; found: 656.0794.

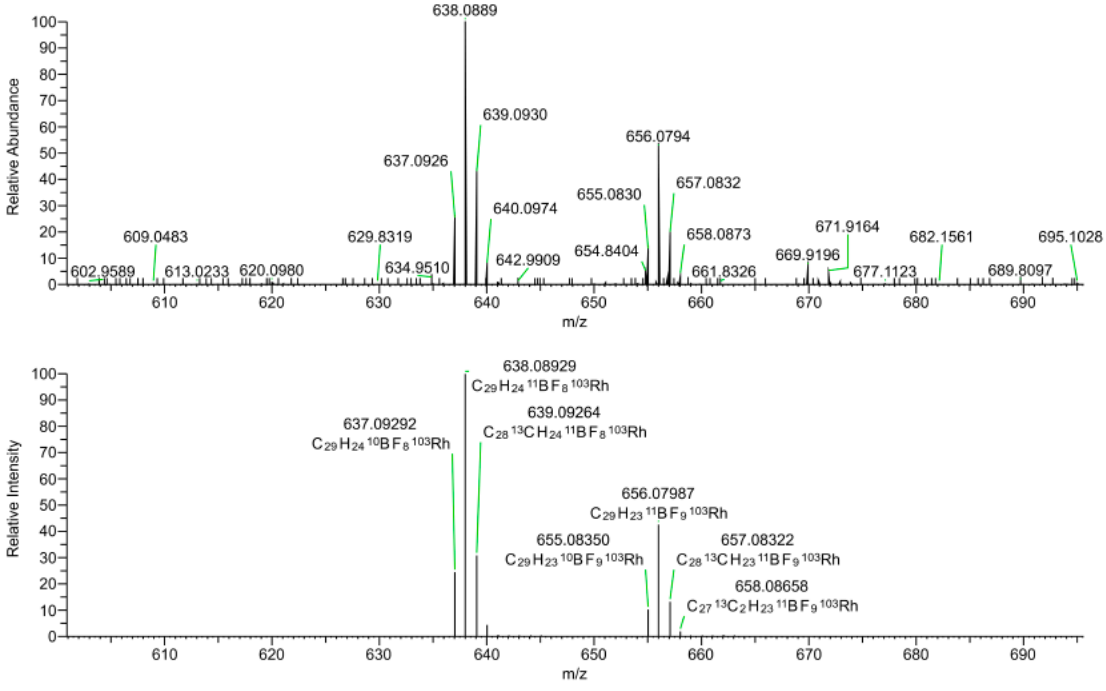

Figure S29. 2-F generated from 1 equiv. $DB(C_6F_5)_2$, Mass Spectrometry - APCI top (experimental), bottom (theoretical) showing an approximately 1:1 ratio of deuterated:non-deuterated sample. a) 100% D theoretical; b) 100% H theoretical; c) 50%D:50%H theoretical; d) 40%D:60%H theoretical. Signals correspond to $[M+H]^+$.

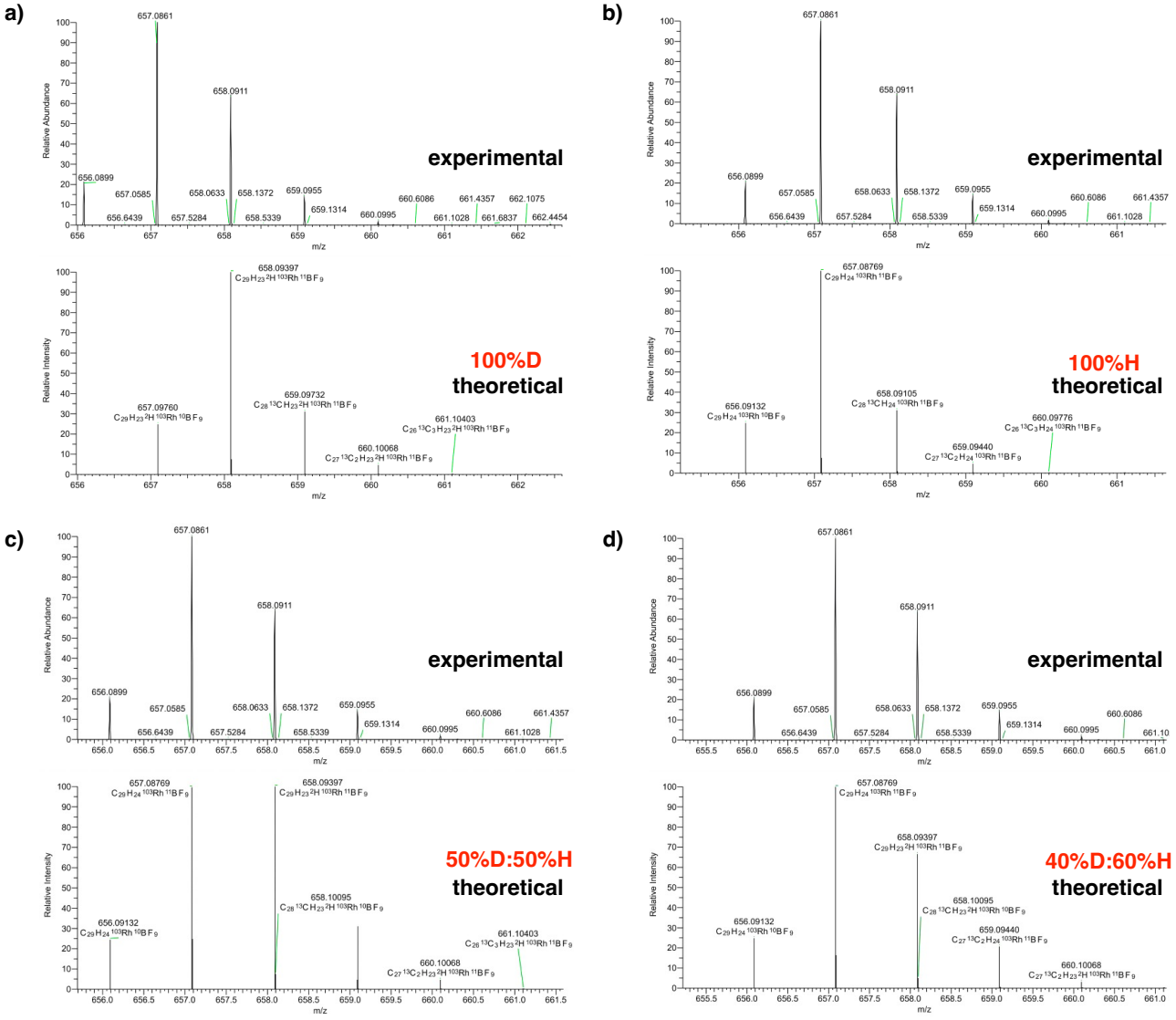

Figure S30. 2-H generated from 1 equiv. $DB(C_6F_5)_2$, Mass Spectrometry - APCI top (experimental), bottom (theoretical) showing an approximately 1:1 ratio of deuterated:non-deuterated sample. a) 100% D theoretical; b) 100% H theoretical; c) 50%D:50%H theoretical; d) 55%D:45%H theoretical. Signals correspond to $[M+H]^+$.

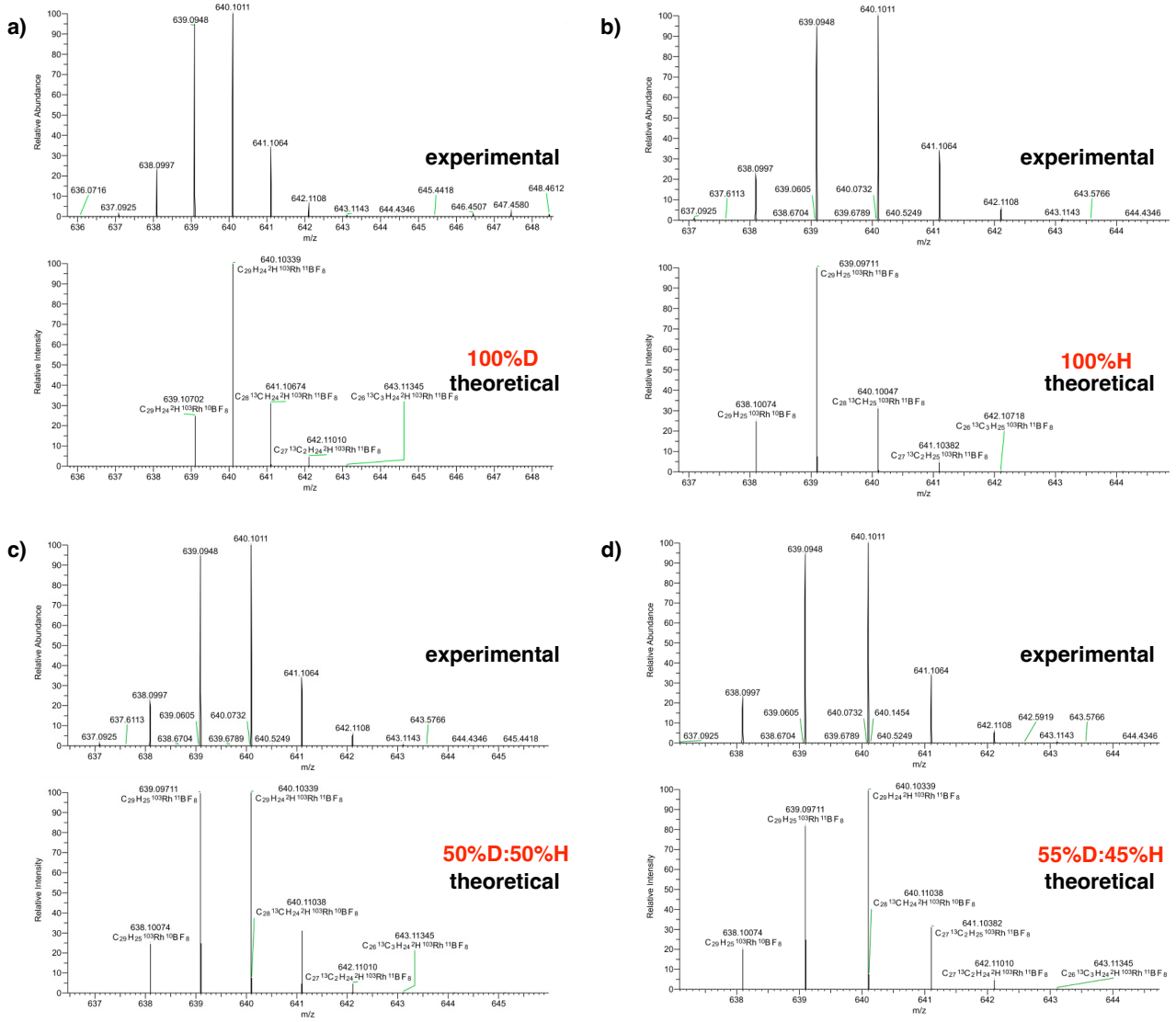

5. X-Ray Crystallography:

Experimental for 2-H/2-F

Data Collection and Processing. The sample was mounted on a Mitegen polyimide micromount with a small amount of Paratone N oil. All X-ray measurements were made on a Bruker Kappa Axis Apex2 diffractometer at a temperature of 110 K. The unit cell dimensions were determined from a symmetry constrained fit of 9723 reflections with $5.86° < 2\theta < 70.98°$. The data collection strategy was a number of φ and ω scans which collected data up to 71.93° (2θ). The frame integration was performed using SAINT.

[4] The data were absorption corrected using a multi-scan empirical absorption method. Scaling and an empirical absorption correction were performed by TWINABS.[5]

Structure Solution and Refinement. The structure was solved by using a dual space methodology using the SHELXT program.[6] All non-hydrogen atoms were obtained from the initial solution. The hydrogen atoms were introduced at idealized positions and were allowed to ride on the parent atom. Although the sample crystal was twinned, the best refinement was obtained using data from only the predominant twin fraction. The structure contained a compositional disorder wherein the terminal atom bound to atom C12 was either F or H. The occupancy for the predominant disorder component (containing the Fluorine atom) refined to a value of 0.592(5). The structural model was fit to the data using full matrix least-squares based on F^2. The calculated structure factors included corrections for anomalous dispersion from the usual tabulation. The structure was refined using the SHELXL program from the SHELX suite of crystallographic software.[7] Graphic plots were produced using the Mercury program.[8] Additional information and other relevant literature references can be found in the reference section of this website (http://xray.chem.uwo.ca).

Routine checkCIF and structure factor analyses were performed using Platon. [9] CCDC **2494566** contains the supplementary crystallographic data for this paper. These data can be obtained free of charge from The Cambridge Crystallographic Data Centre *via* www.ccdc.cam.ac.uk/data_request/cif.

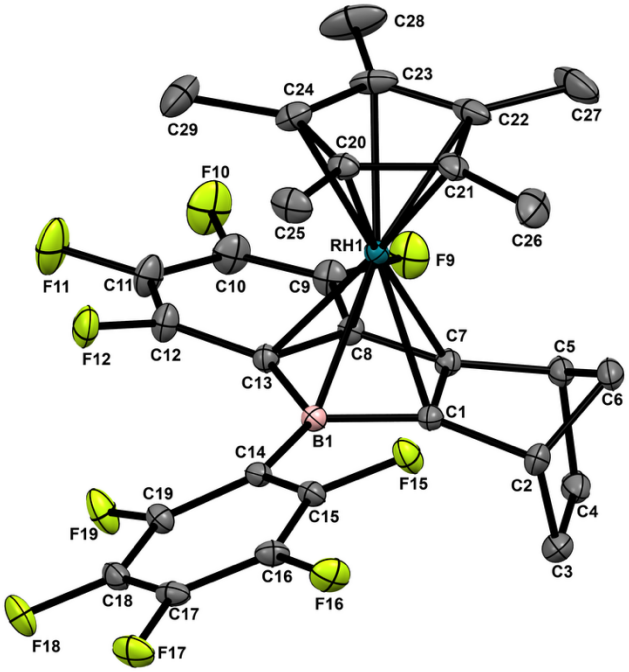

Figure S31. ORTEP drawing of **2-H/2-F** showing naming and numbering scheme. Ellipsoids are at the 50% probability level and hydrogen atoms were omitted for clarity.

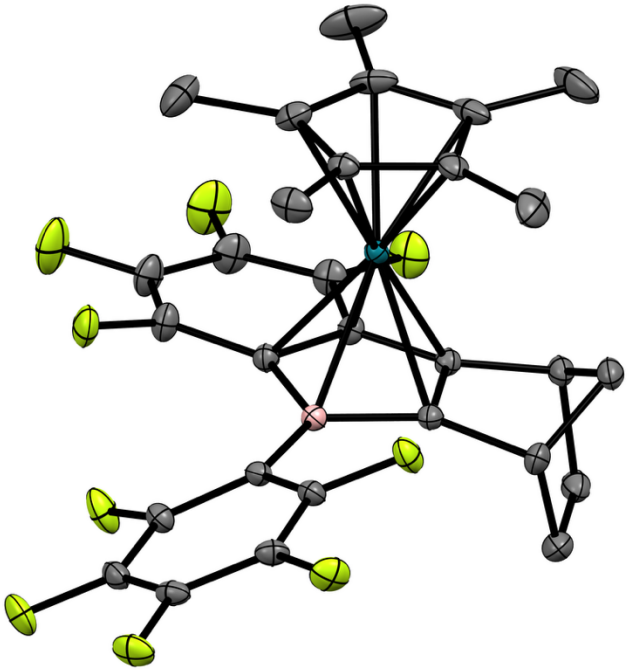

Figure S32. ORTEP drawing of **2-H/2-F**. Ellipsoids are at the 50% probability level and hydrogen atoms were omitted for clarity

Table S1. Summary of Crystal Data for **2-H/2-F**.

Formula	$C_{29}H_{23.41}BF_{8.59}Rh$
Formula Weight (*g*/*mol*)	648.82
Crystal Dimensions (*mm*)	0.249 × 0.128 × 0.075
Crystal Colour and Habit	orange prism
Crystal System	triclinic
Space Group	P -1
Temperature, K	110
a, Å	8.2646(10)
b, Å	9.3254(11)
c, Å	17.716(2)
α,°	88.548(5)
β,°	77.438(6)
γ,°	69.538(4)
V, Å^3	1246.7(3)
Number of reflections to determine final unit cell	9723
Min and Max 2θ for cell determination, °	5.86, 70.98
Z	2
F(000)	649
ϱ (*g*/*cm*^{3})	1.728
λ, Å, (MoKα)	0.71073
μ, (*cm*$^{-1}$)	0.768
Diffractometer Type	Bruker Kappa Axis Apex2
Scan Type(s)	φ and ω scans
Max 2θ for data collection, °	71.93
Measured fraction of data	0.997
Number of reflections measured	11524
Unique reflections measured	11524

R_{merge}	0.0333
Number of reflections included in refinement	11524
Cut off Threshold Expression	$I > 2\sigma(I)$
Structure refined using	full matrix least-squares using F^2
Weighting Scheme	$w=1/[\sigma^2(Fo^2)+(0.0293P)^2]$ where $P=(Fo^2+2Fc^2)/3$
Number of parameters in least-squares	367
R_1	0.0333
wR_2	0.0653
R_1 (all data)	0.0445
wR_2 (all data)	0.0679
GOF	0.958
Maximum shift/error	0.001
Min & Max peak heights on final ΔF Map (e^-/Å)	-0.550, 1.184

Where:

$R_1 = \Sigma \mid |F_o| - |F_c| \mid / \Sigma F_o$

$wR_2 = [\Sigma(w(F_o^2 - F_c^2)^2) / \Sigma(w F_o^4)]^{½}$

GOF = $[\Sigma(w(F_o^2 - F_c^2)^2) / (\text{No. of reflns. - No. of params.})]^{½}$

Table S2. Atomic Coordinates for for **2-H/2-F**.

Atom	x	y	z	$U_{iso/equiv}$
Rh1	0.24071(2)	0.78870(2)	0.22040(2)	0.01081(3)
B1	0.3992(2)	0.70028(16)	0.31341(8)	0.0125(2)
C1	0.29480(18)	0.87280(15)	0.32587(7)	0.0127(2)
C2	0.1686(2)	1.00339(15)	0.38326(8)	0.0163(2)
C3	0.2907(2)	1.07958(17)	0.40813(9)	0.0207(3)
C4	0.3473(2)	1.16152(16)	0.33479(9)	0.0196(3)
C5	0.25657(19)	1.11967(15)	0.27486(8)	0.0160(2)
C6	0.0808(2)	1.12493(16)	0.32925(9)	0.0181(3)

C7	0.34642(18)	0.94869(14)	0.25870(7)	0.0130(2)
C8	0.48559(18)	0.84170(15)	0.20270(7)	0.0135(2)
C9	0.5821(2)	0.86620(17)	0.12962(8)	0.0186(3)
C10	0.7084(2)	0.74584(19)	0.08510(9)	0.0229(3)
C11	0.7379(2)	0.59394(18)	0.10954(9)	0.0229(3)
C12	0.6450(2)	0.56519(16)	0.17771(9)	0.0189(3)
C12'	0.6450(2)	0.56519(16)	0.17771(9)	0.0189(3)
C13	0.52113(18)	0.68702(15)	0.23055(7)	0.0133(2)
F9	0.54938(15)	1.00962(11)	0.10600(6)	0.0278(2)
F10	0.80531(16)	0.76584(13)	0.01708(6)	0.0348(3)
F11	0.86050(16)	0.47886(13)	0.06135(6)	0.0363(3)
F12	0.6631(2)	0.41897(17)	0.19095(9)	0.0239(5)
C14	0.39171(18)	0.57233(15)	0.37356(7)	0.0126(2)
C15	0.24061(19)	0.59260(15)	0.43224(7)	0.0140(2)
C16	0.2338(2)	0.49465(16)	0.49200(7)	0.0156(2)
C17	0.3799(2)	0.36533(16)	0.49363(8)	0.0162(2)
C18	0.5322(2)	0.33838(15)	0.43660(8)	0.0161(2)
C19	0.53554(19)	0.44231(15)	0.37910(8)	0.0146(2)
F15	0.09199(12)	0.71399(10)	0.43397(5)	0.01954(17)
F16	0.08861(13)	0.52579(11)	0.54930(5)	0.02204(18)
F17	0.37456(14)	0.26955(11)	0.55078(5)	0.02286(19)
F18	0.67559(14)	0.21459(11)	0.43787(6)	0.0250(2)
F19	0.69234(13)	0.41360(11)	0.32914(6)	0.0253(2)
C20	0.06441(19)	0.65927(16)	0.21872(8)	0.0146(2)
C21	-0.0374(2)	0.81928(17)	0.23268(9)	0.0174(2)
C22	0.0137(2)	0.89806(18)	0.16546(9)	0.0221(3)
C23	0.1514(2)	0.7872(2)	0.11211(8)	0.0232(3)
C24	0.1841(2)	0.63868(17)	0.14514(8)	0.0184(3)
C25	0.0401(2)	0.53509(18)	0.26991(9)	0.0226(3)

C26	-0.1840(2)	0.8868(2)	0.30265(11)	0.0277(3)
C27	-0.0725(3)	1.0649(2)	0.15275(13)	0.0386(5)
C28	0.2460(4)	0.8134(3)	0.03345(10)	0.0424(6)
C29	0.3127(3)	0.4888(2)	0.10632(11)	0.0302(4)
H2	0.085950	0.975756	0.426255	0.020
H3A	0.225437	1.154174	0.452768	0.025
H3B	0.395068	1.001545	0.422135	0.025
H4A	0.304758	1.273824	0.345509	0.023
H4B	0.477707	1.122990	0.316188	0.023
H5	0.246802	1.183580	0.228727	0.019
H6A	0.005292	1.092143	0.302379	0.022
H6B	0.012850	1.226652	0.356419	0.022
H12'	0.662848	0.462054	0.190491	0.023
H25A	-0.036356	0.490390	0.251483	0.034
H25B	-0.014907	0.578073	0.323089	0.034
H25C	0.155633	0.455389	0.268721	0.034
H26A	-0.286794	0.860026	0.299036	0.042
H26B	-0.217449	0.998573	0.305131	0.042
H26C	-0.143568	0.845874	0.349453	0.042
H27A	-0.170223	1.078089	0.127142	0.058
H27B	0.014947	1.102001	0.120059	0.058
H27C	-0.118458	1.123375	0.202773	0.058
H28A	0.200186	0.778683	-0.006429	0.064
H28B	0.373164	0.755633	0.026156	0.064
H28C	0.226285	0.922907	0.029285	0.064
H29A	0.255289	0.446223	0.074504	0.045
H29B	0.351198	0.417055	0.145722	0.045
H29C	0.415804	0.505233	0.073347	0.045

Table S3. Anisotropic Displacement Parameters for for **2-H/2-F**.

Atom	u^{11}	u^{22}	u^{33}	u^{12}	u^{13}	u^{23}
Rh1	0.01271(5)	0.01016(4)	0.01000(4)	-0.00407(3)	-0.00351(3)	0.00168(3)
B1	0.0120(6)	0.0127(6)	0.0120(6)	-0.0032(5)	-0.0031(5)	0.0006(4)
C1	0.0118(6)	0.0128(5)	0.0131(5)	-0.0034(4)	-0.0036(4)	-0.0009(4)
C2	0.0165(6)	0.0133(5)	0.0158(6)	-0.0017(5)	-0.0022(5)	-0.0033(4)
C3	0.0227(7)	0.0173(6)	0.0216(6)	-0.0031(5)	-0.0094(6)	-0.0039(5)
C4	0.0187(7)	0.0141(6)	0.0265(7)	-0.0038(5)	-0.0093(6)	-0.0019(5)
C5	0.0161(6)	0.0110(5)	0.0211(6)	-0.0032(5)	-0.0069(5)	0.0004(4)
C6	0.0152(6)	0.0137(5)	0.0236(6)	-0.0014(5)	-0.0065(5)	-0.0022(5)
C7	0.0132(6)	0.0114(5)	0.0146(5)	-0.0041(4)	-0.0039(4)	0.0006(4)
C8	0.0137(6)	0.0127(5)	0.0142(5)	-0.0056(4)	-0.0020(4)	0.0005(4)
C9	0.0202(7)	0.0175(6)	0.0187(6)	-0.0094(5)	-0.0013(5)	0.0043(5)
C10	0.0215(7)	0.0270(7)	0.0173(6)	-0.0100(6)	0.0042(5)	0.0013(5)
C11	0.0203(7)	0.0211(7)	0.0201(6)	-0.0038(6)	0.0050(6)	-0.0052(5)
C12	0.0188(7)	0.0140(6)	0.0197(6)	-0.0037(5)	0.0012(5)	-0.0019(5)
C12'	0.0188(7)	0.0140(6)	0.0197(6)	-0.0037(5)	0.0012(5)	-0.0019(5)
C13	0.0126(6)	0.0125(5)	0.0136(5)	-0.0031(4)	-0.0024(4)	0.0002(4)
F9	0.0332(6)	0.0218(4)	0.0275(5)	-0.0131(4)	0.0001(4)	0.0087(4)
F10	0.0351(6)	0.0368(6)	0.0240(5)	-0.0143(5)	0.0138(4)	0.0015(4)
F11	0.0345(6)	0.0279(5)	0.0287(5)	-0.0017(5)	0.0151(5)	-0.0080(4)
F12	0.0291(10)	0.0114(7)	0.0244(8)	-0.0010(6)	-0.0019(6)	-0.0015(5)
C14	0.0133(6)	0.0131(5)	0.0123(5)	-0.0043(4)	-0.0053(4)	0.0013(4)
C15	0.0140(6)	0.0145(5)	0.0131(5)	-0.0034(5)	-0.0052(4)	0.0021(4)
C16	0.0168(6)	0.0200(6)	0.0118(5)	-0.0085(5)	-0.0038(5)	0.0021(4)
C17	0.0229(7)	0.0161(6)	0.0150(5)	-0.0106(5)	-0.0100(5)	0.0056(4)
C18	0.0180(6)	0.0120(5)	0.0197(6)	-0.0039(5)	-0.0095(5)	0.0038(4)
C19	0.0128(6)	0.0147(5)	0.0165(6)	-0.0044(5)	-0.0047(5)	0.0024(4)

F15	0.0136(4)	0.0203(4)	0.0185(4)	0.0000(3)	-0.0013(3)	0.0040(3)
F16	0.0218(5)	0.0298(5)	0.0134(4)	-0.0102(4)	0.0000(3)	0.0036(3)
F17	0.0317(5)	0.0227(4)	0.0205(4)	-0.0139(4)	-0.0126(4)	0.0121(3)
F18	0.0225(5)	0.0167(4)	0.0320(5)	-0.0002(4)	-0.0104(4)	0.0088(3)
F19	0.0129(4)	0.0245(4)	0.0300(5)	0.0002(4)	0.0002(4)	0.0092(4)
C20	0.0158(6)	0.0160(5)	0.0150(5)	-0.0080(5)	-0.0055(5)	0.0028(4)
C21	0.0140(6)	0.0178(6)	0.0221(6)	-0.0046(5)	-0.0092(5)	0.0012(5)
C22	0.0289(8)	0.0197(6)	0.0267(7)	-0.0120(6)	-0.0200(6)	0.0098(5)
C23	0.0361(9)	0.0308(8)	0.0146(6)	-0.0225(7)	-0.0129(6)	0.0087(5)
C24	0.0246(7)	0.0201(6)	0.0138(5)	-0.0119(6)	-0.0048(5)	0.0000(5)
C25	0.0282(8)	0.0227(7)	0.0234(7)	-0.0155(6)	-0.0095(6)	0.0103(5)
C26	0.0128(7)	0.0306(8)	0.0366(9)	-0.0034(6)	-0.0051(6)	-0.0085(7)
C27	0.0521(13)	0.0219(8)	0.0559(12)	-0.0137(8)	-0.0413(11)	0.0180(8)
C28	0.0733(16)	0.0599(13)	0.0154(7)	-0.0488(13)	-0.0126(8)	0.0123(7)
C29	0.0325(9)	0.0294(8)	0.0275(8)	-0.0126(7)	0.0000(7)	-0.0132(6)

Table S4. Bond Lengths for for **2-H/2-F**.

Rh1-C7	2.1611(13)	C12-C13	1.4281(19)
Rh1-C21	2.1769(15)	C12'-C13	1.4281(19)
Rh1-C24	2.1858(14)	C12'-H12'	0.9500
Rh1-C20	2.1980(13)	C14-C19	1.389(2)
Rh1-C23	2.2025(15)	C14-C15	1.3986(19)
Rh1-C8	2.2032(13)	C15-F15	1.3433(17)
Rh1-C22	2.2167(16)	C15-C16	1.3855(18)
Rh1-C13	2.2223(14)	C16-F16	1.3404(16)
Rh1-C1	2.2337(13)	C16-C17	1.381(2)
Rh1-B1	2.2861(15)	C17-F17	1.3368(15)
B1-C1	1.532(2)	C17-C18	1.381(2)

B1-C13	1.5697(19)	C18-F18	1.3383(17)
B1-C14	1.5879(18)	C18-C19	1.3908(18)
C1-C7	1.4306(18)	C19-F19	1.3434(17)
C1-C2	1.5225(19)	C20-C24	1.426(2)
C2-C6	1.549(2)	C20-C21	1.430(2)
C2-C3	1.558(2)	C20-C25	1.4947(18)
C2-H2	1.0000	C21-C22	1.446(2)
C3-C4	1.558(2)	C21-C26	1.501(2)
C3-H3A	0.9900	C22-C23	1.420(3)
C3-H3B	0.9900	C22-C27	1.502(2)
C4-C5	1.554(2)	C23-C24	1.449(2)
C4-H4A	0.9900	C23-C28	1.502(2)
C4-H4B	0.9900	C24-C29	1.500(2)
C5-C7	1.5095(19)	C25-H25A	0.9800
C5-C6	1.544(2)	C25-H25B	0.9800
C5-H5	1.0000	C25-H25C	0.9800
C6-H6A	0.9900	C26-H26A	0.9800
C6-H6B	0.9900	C26-H26B	0.9800
C7-C8	1.4332(19)	C26-H26C	0.9800
C8-C9	1.4242(18)	C27-H27A	0.9800
C8-C13	1.4632(18)	C27-H27B	0.9800
C9-F9	1.3434(17)	C27-H27C	0.9800
C9-C10	1.356(2)	C28-H28A	0.9800
C10-F10	1.3422(17)	C28-H28B	0.9800
C10-C11	1.424(2)	C28-H28C	0.9800
C11-F11	1.3480(18)	C29-H29A	0.9800
C11-C12'	1.358(2)	C29-H29B	0.9800
C11-C12	1.358(2)	C29-H29C	0.9800
C12-F12	1.339(2)		

Table S5. Bond Angles for **2-H/2-F**.

C7-Rh1-C21	127.00(5)	F10-C10-C9	121.48(14)
C7-Rh1-C24	161.11(5)	F10-C10-C11	118.60(14)
C21-Rh1-C24	63.93(6)	C9-C10-C11	119.92(13)
C7-Rh1-C20	160.06(5)	F11-C11-C12'	121.14(14)
C21-Rh1-C20	38.17(5)	F11-C11-C12	121.14(14)
C24-Rh1-C20	37.96(5)	F11-C11-C10	117.07(13)
C7-Rh1-C23	127.59(5)	C12'-C11-C10	121.79(14)
C21-Rh1-C23	63.71(6)	C12-C11-C10	121.79(14)
C24-Rh1-C23	38.56(6)	F12-C12-C11	117.61(14)
C20-Rh1-C23	63.76(5)	F12-C12-C13	120.91(13)
C7-Rh1-C8	38.33(5)	C11-C12-C13	121.27(13)
C21-Rh1-C8	160.51(5)	C11-C12'-C13	121.27(13)
C24-Rh1-C8	126.31(5)	C11-C12'-H12'	119.4
C20-Rh1-C8	159.86(5)	C13-C12'-H12'	119.4
C23-Rh1-C8	112.48(5)	C12'-C13-C8	115.96(11)
C7-Rh1-C22	113.71(5)	C12-C13-C8	115.96(11)
C21-Rh1-C22	38.41(6)	C12'-C13-B1	136.10(12)
C24-Rh1-C22	63.75(6)	C12-C13-B1	136.10(12)
C20-Rh1-C22	63.77(5)	C8-C13-B1	107.86(11)
C23-Rh1-C22	37.48(7)	C12'-C13-Rh1	120.44(11)
C8-Rh1-C22	126.59(5)	C12-C13-Rh1	120.44(11)
C7-Rh1-C13	65.15(5)	C8-C13-Rh1	69.99(8)
C21-Rh1-C13	160.12(5)	B1-C13-Rh1	71.82(8)
C24-Rh1-C13	109.74(6)	C19-C14-C15	114.09(11)
C20-Rh1-C13	125.11(5)	C19-C14-B1	124.41(12)
C23-Rh1-C13	124.32(6)	C15-C14-B1	121.09(12)
C8-Rh1-C13	38.61(5)	F15-C15-C16	116.02(12)

C22-Rh1-C13	158.33(6)	F15-C15-C14	120.31(11)
C7-Rh1-C1	37.95(5)	C16-C15-C14	123.66(13)
C21-Rh1-C1	112.72(5)	F16-C16-C17	119.55(12)
C24-Rh1-C1	158.98(5)	F16-C16-C15	120.76(13)
C20-Rh1-C1	126.13(5)	C17-C16-C15	119.67(13)
C23-Rh1-C1	161.16(6)	F17-C17-C18	120.60(13)
C8-Rh1-C1	64.12(5)	F17-C17-C16	120.20(13)
C22-Rh1-C1	127.89(6)	C18-C17-C16	119.18(12)
C13-Rh1-C1	65.81(5)	F18-C18-C17	119.93(12)
C7-Rh1-B1	65.88(5)	F18-C18-C19	120.71(13)
C21-Rh1-B1	124.92(5)	C17-C18-C19	119.34(13)
C24-Rh1-B1	123.26(6)	F19-C19-C14	120.35(11)
C20-Rh1-B1	109.48(5)	F19-C19-C18	115.59(13)
C23-Rh1-B1	158.43(6)	C14-C19-C18	124.00(13)
C8-Rh1-B1	66.19(5)	C24-C20-C21	107.91(12)
C22-Rh1-B1	160.66(6)	C24-C20-C25	126.23(13)
C13-Rh1-B1	40.72(5)	C21-C20-C25	125.73(13)
C1-Rh1-B1	39.60(5)	C24-C20-Rh1	70.55(8)
C1-B1-C13	102.62(10)	C21-C20-Rh1	70.12(8)
C1-B1-C14	127.24(12)	C25-C20-Rh1	128.05(10)
C13-B1-C14	130.00(12)	C20-C21-C22	108.34(13)
C1-B1-Rh1	68.36(7)	C20-C21-C26	124.20(14)
C13-B1-Rh1	67.46(7)	C22-C21-C26	127.19(15)
C14-B1-Rh1	130.11(10)	C20-C21-Rh1	71.71(8)
C7-C1-C2	103.91(11)	C22-C21-Rh1	72.29(9)
C7-C1-B1	109.55(11)	C26-C21-Rh1	126.48(11)
C2-C1-B1	146.17(12)	C23-C22-C21	107.53(13)
C7-C1-Rh1	68.28(7)	C23-C22-C27	126.57(16)
C2-C1-Rh1	126.98(10)	C21-C22-C27	125.78(17)

B1-C1-Rh1	72.05(8)	C23-C22-Rh1	70.72(9)
C1-C2-C6	102.20(11)	C21-C22-Rh1	69.31(8)
C1-C2-C3	104.31(12)	C27-C22-Rh1	128.37(12)
C6-C2-C3	99.85(11)	C22-C23-C24	108.26(12)
C1-C2-H2	116.1	C22-C23-C28	127.36(17)
C6-C2-H2	116.1	C24-C23-C28	124.35(18)
C3-C2-H2	116.1	C22-C23-Rh1	71.80(9)
C4-C3-C2	103.65(12)	C24-C23-Rh1	70.10(8)
C4-C3-H3A	111.0	C28-C23-Rh1	125.32(13)
C2-C3-H3A	111.0	C20-C24-C23	107.89(13)
C4-C3-H3B	111.0	C20-C24-C29	126.17(13)
C2-C3-H3B	111.0	C23-C24-C29	125.82(14)
H3A-C3-H3B	109.0	C20-C24-Rh1	71.48(8)
C5-C4-C3	103.45(11)	C23-C24-Rh1	71.35(8)
C5-C4-H4A	111.1	C29-C24-Rh1	125.78(12)
C3-C4-H4A	111.1	C20-C25-H25A	109.5
C5-C4-H4B	111.1	C20-C25-H25B	109.5
C3-C4-H4B	111.1	H25A-C25-H25B	109.5
H4A-C4-H4B	109.0	C20-C25-H25C	109.5
C7-C5-C6	99.96(10)	H25A-C25-H25C	109.5
C7-C5-C4	105.00(12)	H25B-C25-H25C	109.5
C6-C5-C4	99.58(12)	C21-C26-H26A	109.5
C7-C5-H5	116.6	C21-C26-H26B	109.5
C6-C5-H5	116.6	H26A-C26-H26B	109.5
C4-C5-H5	116.6	C21-C26-H26C	109.5
C5-C6-C2	95.38(11)	H26A-C26-H26C	109.5
C5-C6-H6A	112.7	H26B-C26-H26C	109.5
C2-C6-H6A	112.7	C22-C27-H27A	109.5
C5-C6-H6B	112.7	C22-C27-H27B	109.5

C2-C6-H6B	112.7	H27A-C27-H27B	109.5
H6A-C6-H6B	110.2	C22-C27-H27C	109.5
C1-C7-C8	110.66(11)	H27A-C27-H27C	109.5
C1-C7-C5	108.94(11)	H27B-C27-H27C	109.5
C8-C7-C5	139.47(12)	C23-C28-H28A	109.5
C1-C7-Rh1	73.78(7)	C23-C28-H28B	109.5
C8-C7-Rh1	72.43(7)	H28A-C28-H28B	109.5
C5-C7-Rh1	127.97(10)	C23-C28-H28C	109.5
C9-C8-C7	130.25(12)	H28A-C28-H28C	109.5
C9-C8-C13	120.57(12)	H28B-C28-H28C	109.5
C7-C8-C13	109.18(11)	C24-C29-H29A	109.5
C9-C8-Rh1	124.80(11)	C24-C29-H29B	109.5
C7-C8-Rh1	69.24(7)	H29A-C29-H29B	109.5
C13-C8-Rh1	71.40(7)	C24-C29-H29C	109.5
F9-C9-C10	120.44(12)	H29A-C29-H29C	109.5
F9-C9-C8	119.43(13)	H29B-C29-H29C	109.5
C10-C9-C8	120.12(13)		

6. Computational Details:

6.1 Methodology:

Calculations were performed using version 6.0.1 of the ORCA package.[10] All geometry optimizations and frequency calculations were performed at the r^{2}SCAN-3c level of theory, which includes a basis set of triple-zeta quality and empirical corrections to account for dispersion.[11] Frequency calculations were performed to confirm the nature of each stationary point, with transition states having one imaginary frequency and minima having none.

Electronic energies were refined using single point calculations with the TIGHTSCF keyword at the r^{2}SCAN0-D4/ma-Def2-QZVP/SMD(toluene) level of theory.[12] Free energies are calculated from the electronic energy at the higher level of theory plus the correction to free energy from the lower level of theory, plus a correction (+ 1.89 kcal/mol) to account for a standard state of 1 mol L^{-1} rather than 1 atm.[13] i.e.:

$$G \text{ (in kcal/mol)} = E(r^2SCAN0/ma\text{-}Def2\text{-}QZVP/SMD(toluene)) + G_{corr}(r^2SCAN\text{-}3c) + 1.89$$

In each Figure and Scheme, the free energy at r^{2}SCAN-3c is also given, in parentheses, for comparison.

All transition states were checked using IRC calculations to ensure that these linked the anticipated intermediates before and after the transition state.

NBO calculations were carried out using NBO7.[14] QTAIM calculations were carried out using AIMAll.[15]

6.2 Reaction Profile:

The most reasonable reaction mechanism is displayed in **Figures S33** and **S34**. However, we note concerns regarding the very large energy differences between **E** and **TS-K-L**, due to the stability of the former and the need for reductive elimination from rhodium(III) in the latter.

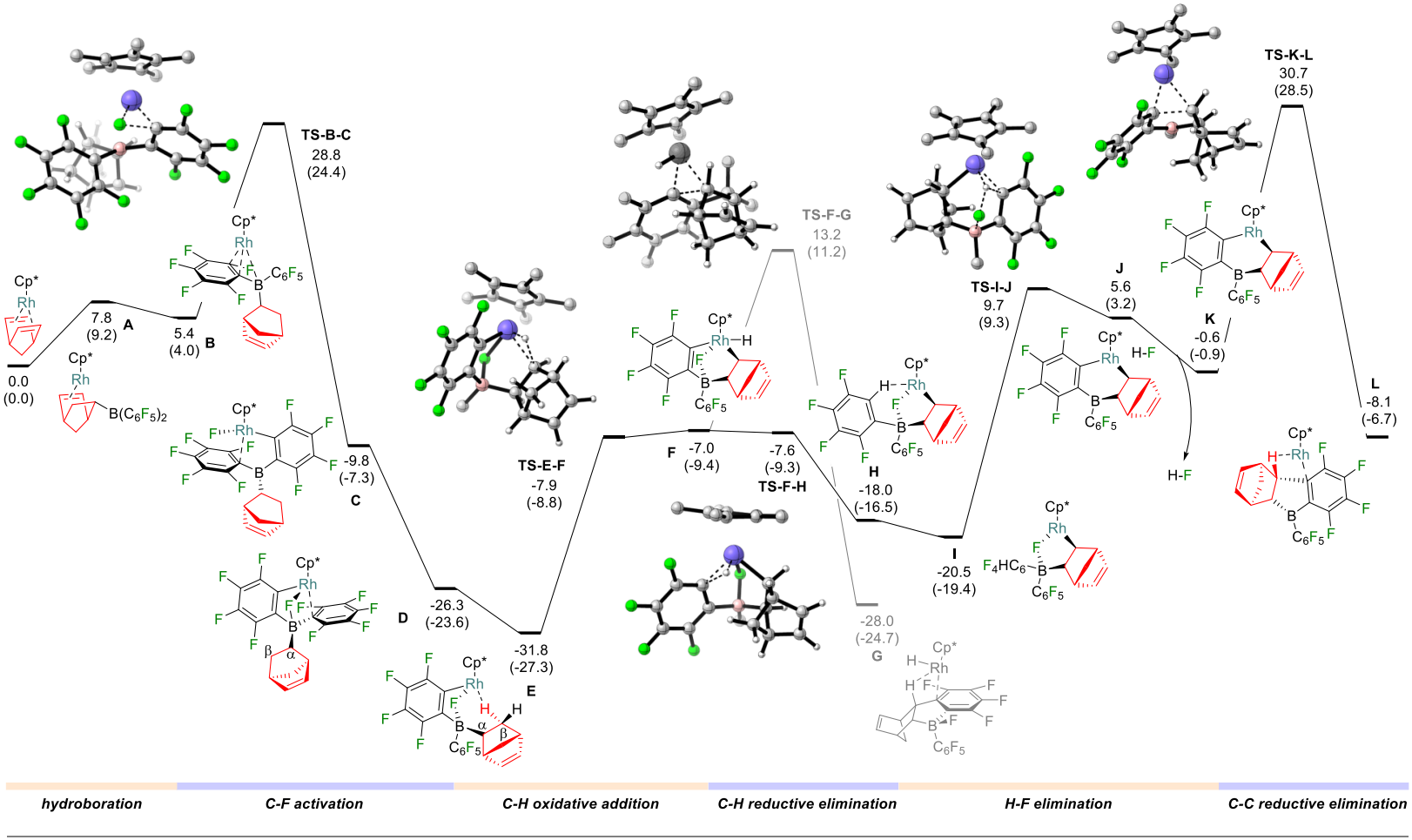

Figure S33. Proposed reaction mechanism (part 1 of 2).

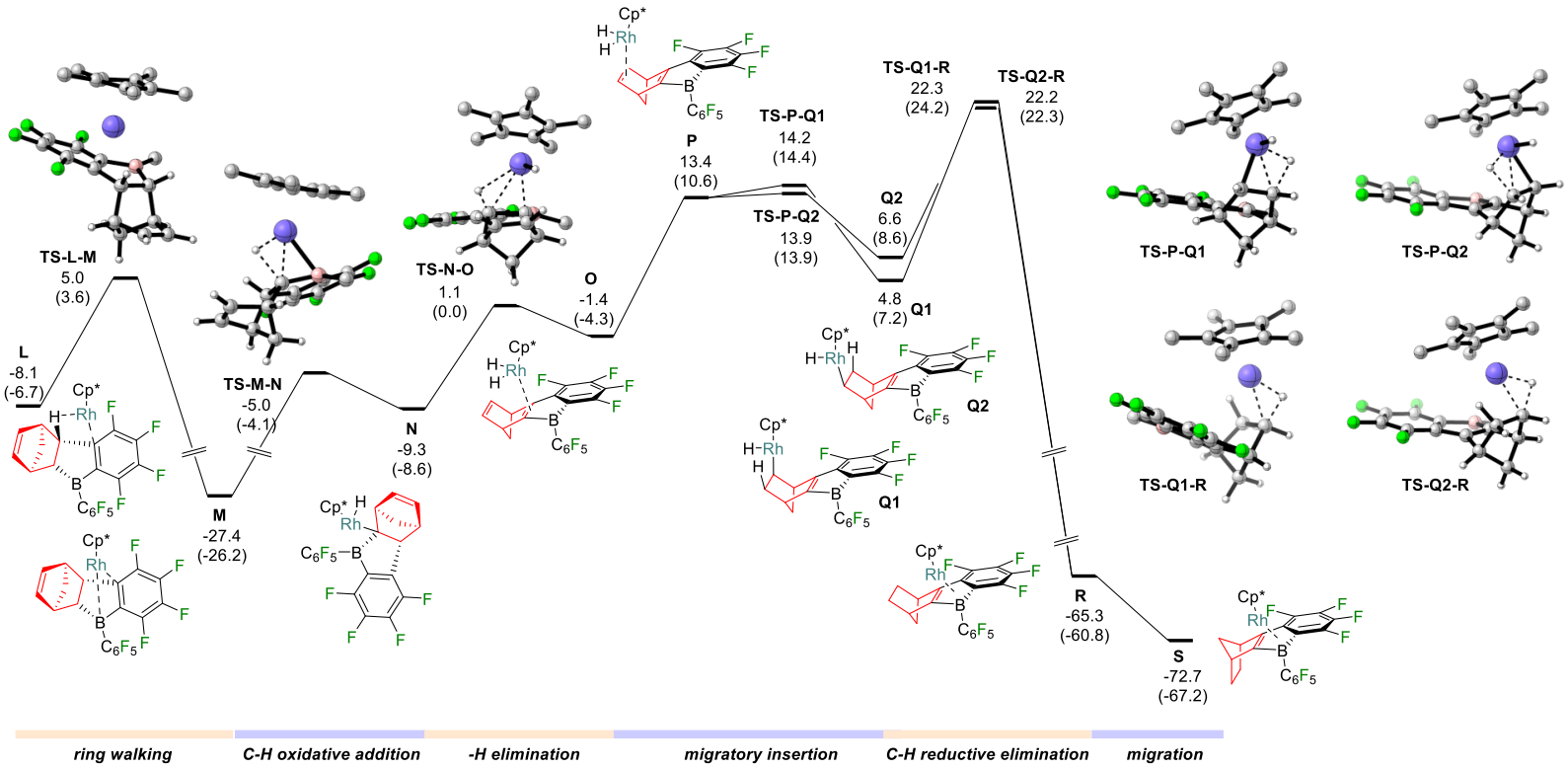

Figure S34. Proposed reaction mechanism (part 2 of 2)

6.3 Kinetic isotope effects:

Kinetic isotope effects were obtained by recalculating the vibrational frequencies of key structures with the atomic mass of the relevant proton set to 2.0141. **Figure S35** displays the overlaid free energy profiles for the d_0 and d_1 structures from **E** to **J**. Kinetic isotope effects are calculated for **TS-E-F**, **TS-F-H**, and **TS-I-J**. No equilibrium isotope effects (EIE) were identified; the energy differences between the d_0 and d_1 intermediates are 1.7-1.8 kcal mol^{-1} in each case.

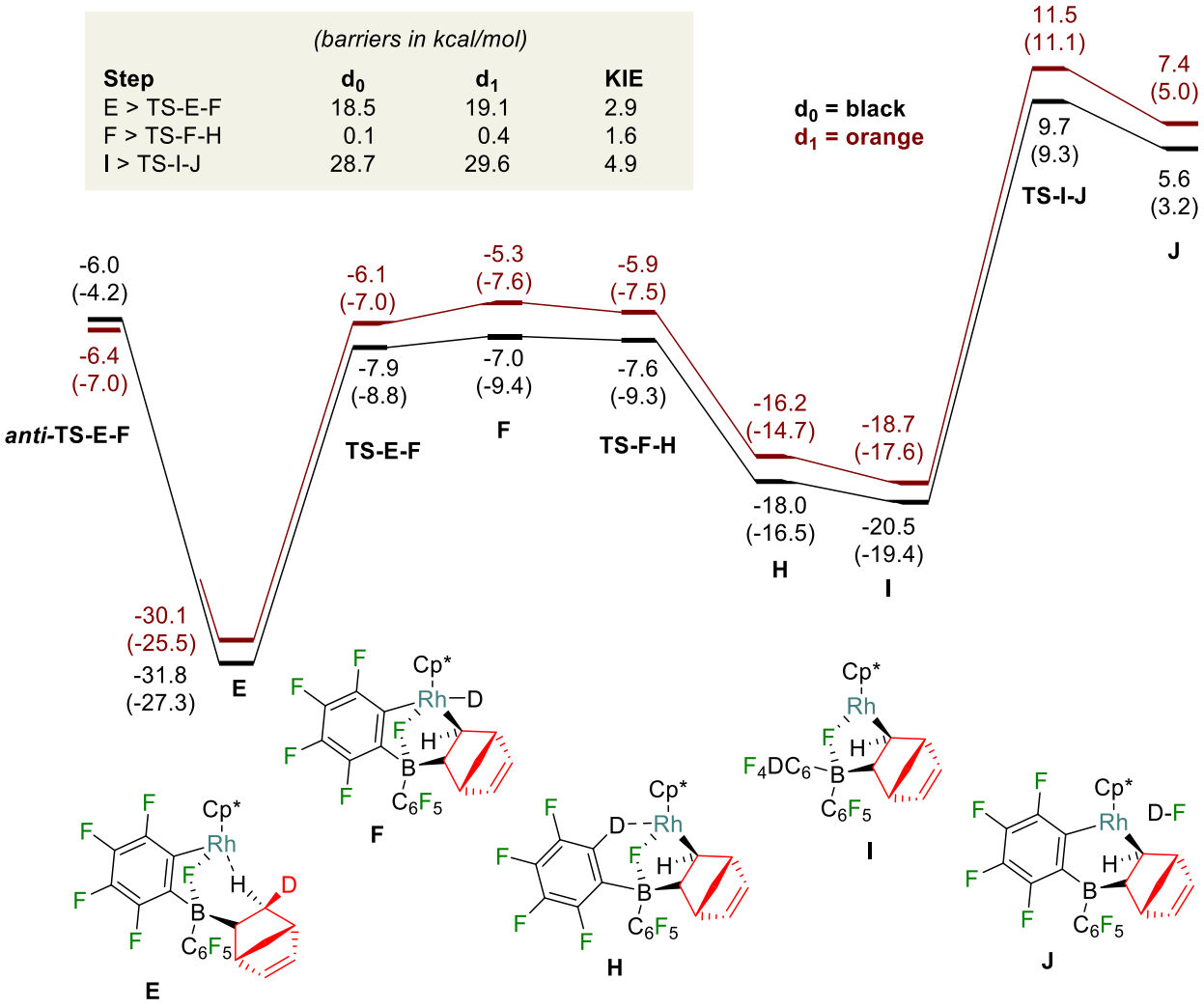

Figure S35. Kinetic isotope effect modelling.

6.4 Alternative reaction profiles:

A series of alternative mechanisms were also modelled.

- Rhodium-catalyzed hydroboration was considered, but this is unfeasible; attempts to locate [Rh(Cp*)(H)(B(C_6F_5)$_2$)] gave an η^2-complex (G_{rel} = 27.0 kcal mol^{-1}). An unfeasible TS for C-F activation at HB(C_6F_5)$_2$ was also ruled out ($\Delta G^{\ddagger}$ = 51.1 kcal mol^{-1}).
- As shown in **Figure S36**, Complex **G** can progress to **T** *via* C-H oxidative addition. **T** is unable to undergo a further C-H insertion (**TS-T-U** is prohibitively high in energy). Dihydrogen reductive elimination *via* **TS-T-V** is facile and exergonic. Complex **V** might then eliminate HF *via* **TS-V-W** but dissociation of dihydrogen to give **X** is much more favourable, and **X** can then progress to the very thermodynamically stable complex **Y**. Similarly, HF elimination from **Y** (*via* **TS-Y-Z**) is feasible, but less favourable than C-H insertion *via* **TS-Y-AA** to give **AA**.
- **Figure S37** shows a series of potential pathways from **AA**. Migratory insertion is facile, and can occur with either regioselectivity. **TS-AA-AB** leads to the isomer where the rhodium sits furthest from boron (**AB**). Binding dihydrogen, which was released from **V** as discussed above, gives **AC** which can then progress *via* hydrogenolysis of the Rh-C bond – without a rhodium dihydride intermediate – to **AD**. Formally, this would then need to eliminate HF to generate the product.
- Formation of the alternative regioisomers of the migratory insertion product without (**AE**) and with bound hydrogen (**AF**) is somewhat more favourable. If **AF** then undergoes HF elimination in concert with H-H activation, this would generate **AG**. After loss of HF – which would most likely be irreversible under the reaction conditions in a borosilicate glass vessel – to give **AH**, reductive elimination would give **AI**, from which rhodium can move across to form **R** and then ultimately **S** (see **Figure S34**, above).
- However, the most favorable process from **AF** is **TS-AF-AJ** – hydrogenolysis of the Rh-C bond – which is followed immediately by migratory insertion to give **AJ**, which is a very stable structure, and which renders the process *via* **TS-AF-AJ** irreversible. Despite repeated attempts and careful analysis of the IRC for this TS, a structure like **AD** could not be located.

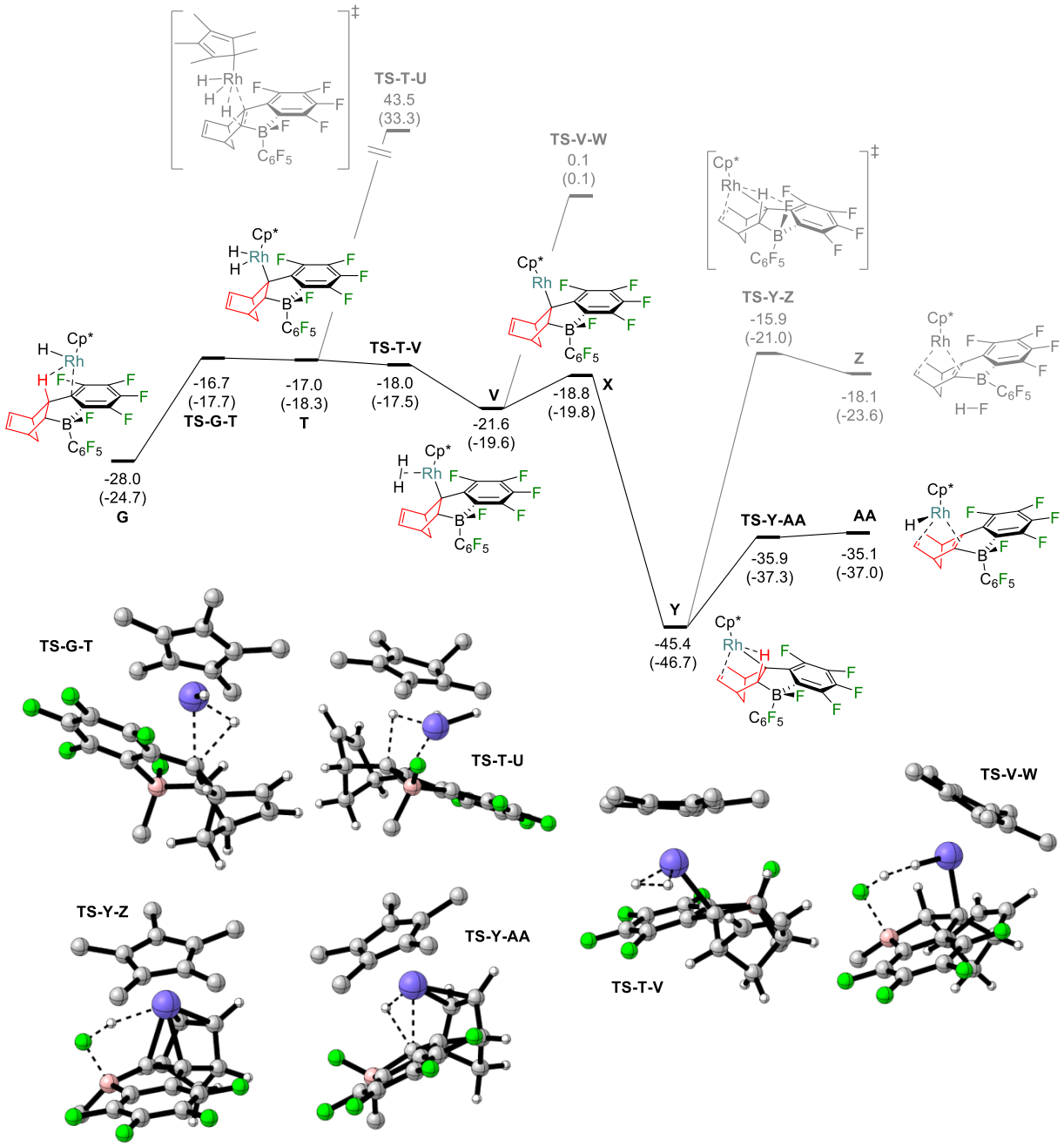

Figure S36. Alternative pathways explored in search of a reaction mechanism (part 1 of 2).

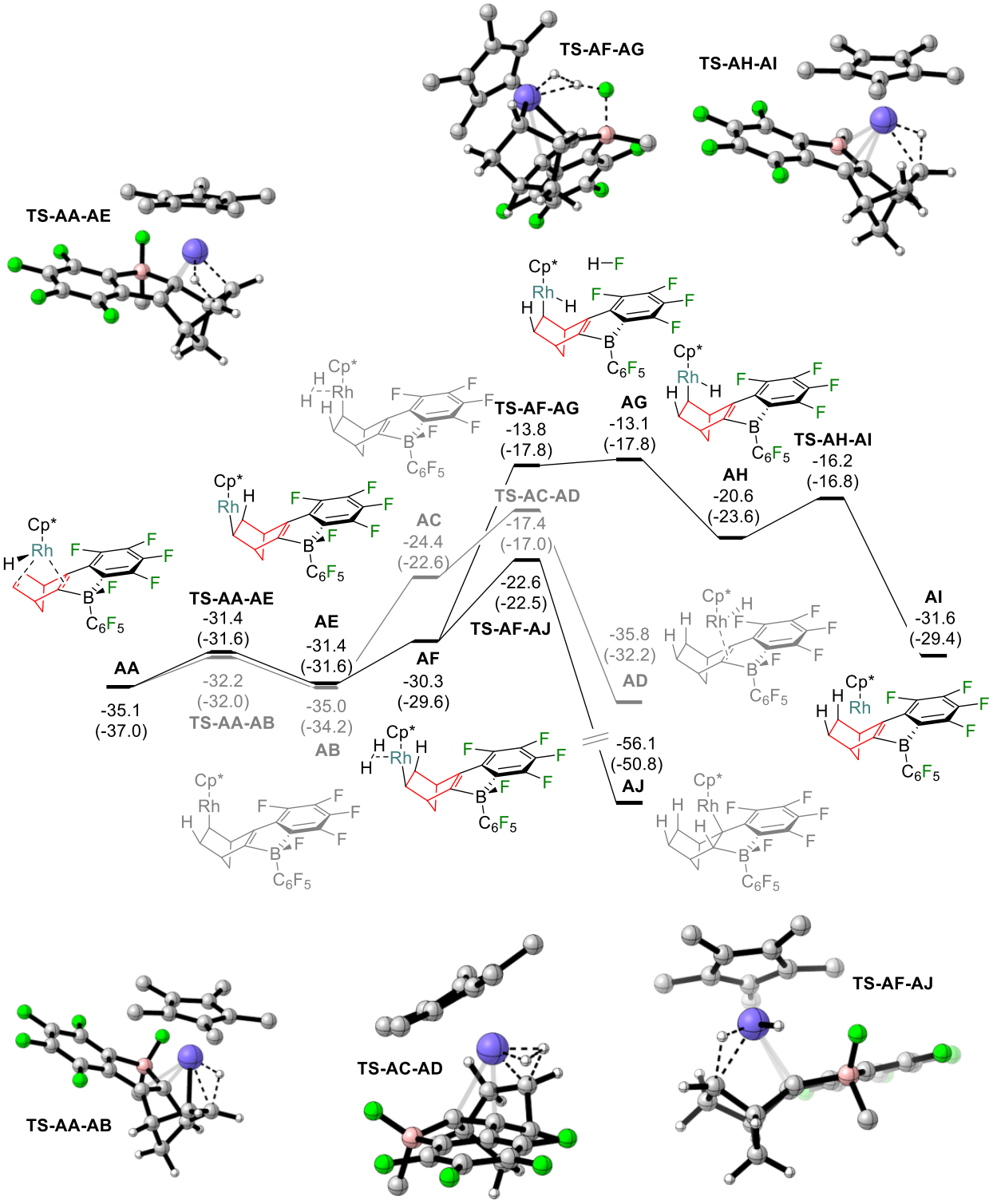

Figure S37. Alternative pathways explored in search of a reaction mechanism (part 2 of 2).

6.5 Table of energies:

Table S6. Table of Energies. Rows in blue refer to structures on the proposed reaction mechanism (**Figures S33** and **S34**). Rows in yellow refer to structures that were obtained as a result of exploring alternative reaction mechanisms (**Figures S36** and **S37**). The corresponding imaginary frequency is tabulated for all transition states.

	r²SCAN-3c OPT FREQ					r²SCAN0-D4/ma-Def2-QZVP/SMD(toluene) SP TIGHTSCF				
	v	Hartrees		kcal/mol		Hartrees		kcal/mol		
Structure	(cm^{-1})	G	G_{corr}	G	G_{rel}	E	G	G	G'	G'_{rel}
(Cp*)Rh(nbd)		-771.816930	0.305100	-484322.4	0.0	-772.103486	-771.798386	-484310.8	-484308.9	0.0
$HB(C_6F_5)_2$		-1480.942622	0.066238	-929305.5		-1480.915342	-1480.849104	-929246.8	-929245.0	
nbd		-271.305563	0.099809	-170246.8		-271.415953	-271.316144	-170253.5	-170251.6	
$(Cp^*)Rh(HB(C_6F_5)_2)$		-1981.413027	0.274043	-1243355.4	25.7	-1981.562392	-1981.288349	-1243277.2	-1243275.3	27.0
A		-2252.744878	0.399742	-1413618.8	9.2	-2253.031747	-2252.632006	-1413547.9	-1413546.0	7.8
B		-2252.753131	0.402311	-1413623.9	4.0	-2253.038114	-2252.635803	-1413550.3	-1413548.4	5.4
TS-B-C	231i	-2252.720663	0.400099	-1413603.6	24.4	-2252.998700	-2252.598601	-1413527.0	-1413525.1	28.8
C		-2252.771173	0.399212	-1413635.3	-7.3	-2253.059386	-2252.660175	-1413565.6	-1413563.7	-9.8
D		-2252.797155	0.403358	-1413651.6	-23.6	-2253.089692	-2252.686334	-1413582.0	-1413580.1	-26.3
E		-2252.803033	0.400949	-1413655.2	-27.3	-2253.096163	-2252.695214	-1413587.6	-1413585.7	-31.8
TS-E-F	444i	-2252.773559	0.398229	-1413636.8	-8.8	-2253.055307	-2252.657079	-1413563.7	-1413561.8	-7.9
anti-TS-E-F	350i	-2252.766262	0.397825	-1413632.2	-4.2	-2253.051890	-2252.654066	-1413561.8	-1413559.9	-6.0
F		-2252.774533	0.398906	-1413637.4	-9.4	-2253.054599	-2252.655693	-1413562.8	-1413560.9	-7.0
TS-F-G	121i	-2252.741684	0.398849	-1413616.7	11.2	-2253.022364	-2252.623515	-1413542.6	-1413540.7	13.2
G		-2252.798913	0.399270	-1413652.7	-24.7	-2253.088329	-2252.689059	-1413583.7	-1413581.8	-28.0
TS-F-H	441i	-2252.774388	0.397945	-1413637.3	-9.3	-2253.054613	-2252.656668	-1413563.4	-1413561.5	-7.6
H		-2252.785839	0.401794	-1413644.5	-16.5	-2253.074942	-2252.673148	-1413573.7	-1413571.9	-18.0
I		-2252.790394	0.402487	-1413647.3	-19.4	-2253.079576	-2252.677089	-1413576.2	-1413574.3	-20.5
TS-I-J	660i	-2252.744729	0.397012	-1413618.7	9.3	-2253.025953	-2252.628942	-1413546.0	-1413544.1	9.7
J		-2252.754486	0.398934	-1413624.8	3.2	-2253.034421	-2252.635488	-1413550.1	-1413548.2	5.6
hydrogen fluoride		-100.451321	-0.007035	-63034.2		-100.444734	-100.451769	-63034.4	-63032.5	

Structure	*v* (cm^{-1})	Hartrees G	Hartrees G_{corr}	kcal/mol G	kcal/mol G_{rel}	Hartrees E	Hartrees G	kcal/mol G	kcal/mol G'	kcal/mol G'_{rel}
K		-2152.309650	0.388687	-1350594.7	-0.9	-2152.585418	-2152.196731	-1350523.8	-1350521.9	-0.6
TS-K-L	412i	-2152.262744	0.386943	-1350565.3	28.5	-2152.533793	-2152.146850	-1350492.5	-1350490.6	30.7
L		-2152.318872	0.388599	-1350600.5	-6.7	-2152.597212	-2152.208614	-1350531.3	-1350529.4	-8.1
TS-L-M	216i	-2152.302442	0.388034	-1350590.2	3.6	-2152.575820	-2152.187786	-1350518.2	-1350516.3	5.0
M		-2152.349956	0.390565	-1350620.0	-26.2	-2152.630019	-2152.239454	-1350550.6	-1350548.8	-27.4
TS-M-N	412i	-2152.314768	0.386112	-1350597.9	-4.1	-2152.589809	-2152.203697	-1350528.2	-1350526.3	-5.0
N		-2152.321941	0.386865	-1350602.4	-8.6	-2152.597419	-2152.210555	-1350532.5	-1350530.6	-9.3
TS-N-O	679i	-2152.308221	0.383700	-1350593.8	0.0	-2152.577720	-2152.194020	-1350522.1	-1350520.2	1.1
O		-2152.315151	0.384650	-1350598.1	-4.3	-2152.582531	-2152.197881	-1350524.6	-1350522.7	-1.4
P		-2152.291391	0.383956	-1350583.2	10.6	-2152.558356	-2152.174400	-1350509.8	-1350507.9	13.4
TS-P-Q1	640i	-2152.285324	0.383593	-1350579.4	14.4	-2152.556613	-2152.173019	-1350509.0	-1350507.1	14.2
Q1		-2152.296771	0.386874	-1350586.6	7.2	-2152.574950	-2152.188076	-1350518.4	-1350516.5	4.8
TS-P-Q2	653i	-2152.286096	0.383244	-1350579.9	13.9	-2152.556815	-2152.173571	-1350509.3	-1350507.4	13.9
Q2		-2152.294507	0.386246	-1350585.2	8.6	-2152.571528	-2152.185282	-1350516.7	-1350514.8	6.6
TS-Q1-R	786i	-2152.269607	0.385249	-1350569.6	24.2	-2152.545420	-2152.160170	-1350500.9	-1350499.0	22.3
TS-Q2-R	795i	-2152.272674	0.384539	-1350571.5	22.3	-2152.544846	-2152.160307	-1350501.0	-1350499.1	22.2
R		-2152.405142	0.393817	-1350654.6	-60.8	-2152.693611	-2152.299794	-1350588.5	-1350586.6	-65.3
S		-2152.415314	0.393440	-1350661.0	-67.2	-2152.705008	-2152.311568	-1350595.9	-1350594.0	-72.7
TS-G-T	98i	-2252.787792	0.396332	-1413645.7	-17.7	-2253.067485	-2252.671153	-1413572.5	-1413570.6	-16.7
T		-2252.788727	0.395427	-1413646.3	-18.3	-2253.066953	-2252.671526	-1413572.7	-1413570.8	-17.0
TS-T-U	710i	-2252.706484	0.390130	-1413594.7	33.3	-2252.965290	-2252.575160	-1413512.3	-1413510.4	43.5
TS-T-V	585i	-2252.788209	0.395547	-1413645.9	-18.0	-2253.067897	-2252.672351	-1413573.2	-1413571.4	-17.5
V		-2252.790795	0.397539	-1413647.6	-19.6	-2253.076459	-2252.678920	-1413577.4	-1413575.5	-21.6
TS-V-W	137i	-2252.759371	0.396567	-1413627.8	0.1	-2253.040947	-2252.644379	-1413555.7	-1413553.8	0.1
W		-2252.762965	0.395243	-1413630.1	-2.1	-2253.043926	-2252.648683	-1413558.4	-1413556.5	-2.6
X		-2251.619811	0.379840	-1412912.8	-19.8	-2251.884542	-2251.504703	-1412840.5	-1412838.6	-18.8
Y		-2251.662656	0.380422	-1412939.6	-46.7	-2251.927446	-2251.547024	-1412867.1	-1412865.2	-45.4
TS-Y-Z	637i	-2251.621735	0.375965	-1412914.0	-21.0	-2251.875976	-2251.500011	-1412837.6	-1412835.7	-15.9
Z		-2251.625892	0.378425	-1412916.6	-23.6	-2251.881904	-2251.503480	-1412839.8	-1412837.9	-18.1

	ν	Hartrees		kcal/mol		Hartrees		kcal/mol		
Structure	(cm^{-1})	**G**	**G_{corr}**	**G**	**G_{rel}**	**E**	**G**	**G**	**G'**	**G'_{rel}**
TS-Y-AA	302i	-2251.647723	0.378280	-1412930.3	-37.3	-2251.910138	-2251.531858	-1412857.6	-1412855.7	-35.9
AA		-2251.647268	0.379018	-1412930.0	-37.0	-2251.909673	-2251.530654	-1412856.8	-1412854.9	-35.1
TS-AA-AB	674i	-2251.639309	0.378095	-1412925.0	-32.0	-2251.904111	-2251.526015	-1412853.9	-1412852.0	-32.2
AB		-2251.642725	0.380219	-1412927.1	-34.2	-2251.910617	-2251.530398	-1412856.7	-1412854.8	-35.0
AC		-2252.795601	0.398254	-1413650.6	-22.6	-2253.081650	-2252.683396	-1413580.2	-1413578.3	-24.4
TS-AC-AD	551i	-2252.786693	0.397139	-1413645.0	-17.0	-2253.069266	-2252.672127	-1413573.1	-1413571.2	-17.4
AD		-2252.810896	0.400481	-1413660.2	-32.2	-2253.101933	-2252.701452	-1413591.5	-1413589.6	-35.8
TS-AA-AE	670i	-2251.638664	0.377736	-1412924.6	-31.6	-2251.902449	-2251.524712	-1412853.1	-1412851.2	-31.4
AE		-2251.643920	0.379985	-1412927.9	-34.9	-2251.910260	-2251.530275	-1412856.6	-1412854.7	-34.9
AF		-2252.806659	0.397748	-1413657.5	-29.6	-2253.090525	-2252.692777	-1413586.1	-1413584.2	-30.3
TS-AF-AG	230i	-2252.787903	0.396854	-1413645.8	-17.8	-2253.063287	-2252.666433	-1413569.5	-1413567.6	-13.8
AG		-2252.787968	0.399139	-1413645.8	-17.8	-2253.064459	-2252.665319	-1413568.8	-1413566.9	-13.1
AH		-2152.345753	0.389683	-1350617.4	-23.5	-2152.618241	-2152.228557	-1350543.8	-1350541.9	-20.6
TS-AH-AI	737i	-2152.334953	0.388604	-1350610.6	-16.8	-2152.610181	-2152.221577	-1350539.4	-1350537.5	-16.2
AI		-2152.355098	0.390232	-1350623.2	-29.4	-2152.636304	-2152.246071	-1350554.8	-1350552.9	-31.6
TS-AF-AJ	597i	-2252.795377	0.396338	-1413650.4	-22.5	-2253.076887	-2252.680549	-1413578.4	-1413576.5	-22.6
AJ		-2252.840476	0.403019	-1413678.7	-50.8	-2253.136832	-2252.733813	-1413611.8	-1413609.9	-56.1
dihydrogen		-1.171278	-0.001896	-735.0		-1.170894	-1.172790	-735.9	-734.0	
TS for $HB(C_6F_5)_2$ C-F activation	233i	-1981.380405	0.27188849	-1243335.0	46.2	-1981.521853	-1981.249964	-1243253.1	-1243251.2	51.1

6.5 Alternative levels of theory

Different levels of theory were benchmarked for TS-B-C *vs* [Rh(Cp*)(nbd)] plus $HB(C_6F_4)_2$. These all give energies within a reasonably narrow range, apart from M06 which gives an unfeasibly high barrier.

Basis Set	Functional	[Rh(Cp*)(nbd)]	$HB(C_6F_5)_2$	TS-B-C	$\Delta G^{\ddagger}$
		E	E	E	
ma-def2-QZVP	r2SCAN0-D4	-772.103486	-1480.915342	-2252.998700	28.8
ma-def2-QZVP	wr2SCAN-D4	-772.260778	-1481.018631	-2253.261183	27.6
ma-def2-QZVP	wB97M-V	-772.162501	-1481.411983	-2253.558415	26.2
ma-def2-QZVP	CAM-B3LYP-D4	-772.146779	-1481.335905	-2253.468508	25.1
ma-def2-QZVP	M06	-772.060257	-1481.112350	-2253.133727	40.6
ma-def2-QZVP	PBE0-D4	-771.791050	-1480.295646	-2252.068057	27.9
ma-def2-QZVP	TPSS0-D4	-772.540696	-1481.565114	-2254.085726	28.8
ma-def2-QZVP	wB97X-D4rev	-772.933419	-1482.019153	-2254.933467	28.1
def2-TZVPD	r2SCAN0-D4	-772.057788	-1480.851208	-2252.890400	27.8
def2-QZVPD	r2SCAN0-D4	-772.103646	-1480.915531	-2252.999119	28.7
def2-QZVPP	r2SCAN0-D4	-772.103737	-1480.914790	-2252.998579	28.7
def2-QZVPPD	r2SCAN0-D4	-772.103956	-1480.915531	-2252.999457	28.7

6.6 XYZ coordinates:

The XYZ coordinates are available:

(1) As a separate supporting information file, from the journal website.

7. References:

[1] G. Smits, B. Audic, M.D. Wodrich, C. Corminboueg, N. Cramer, *Chem. Sci.* **2017**, *8*, 7174.

[2] J. N. Bentley, E. Pradhan, T. Zeng, C. B. Caputo, *Dalton Trans.* **2020**, *49*, 16054.

[3] a) H.C. Brown, S.K. Gupta *J. Am. Chem. Soc.* **1975**, *97*, 5249; b) I. Peuser, R. C. Neu, X. Zhao, M. Ulrich, B. Schirmer, J. A. Tannert, G. Kehr, R. Frohlich, S. Grimme, G. Erker, D. W. Stephan *Chem. Eur. J.* **2011**, *17*, 9640.

[4] Bruker-AXS, SAINT version 2013.8, **2013**, Bruker-AXS, Madison, WI 53711, USA

[5] Bruker-AXS, TWINABS version 2012.1, **2012**, Bruker-AXS, Madison, WI 53711, USA

[6] Sheldrick, G. M., *Acta Cryst.* **2015**, *A71*, 3-8

[7] Sheldrick, G. M., *Acta Cryst.* **2015**, *C71*, 3-8

[8] Macrae, C. F.; Bruno, I. J.; Chisholm, J. A.; Edington, P. R.; McCabe, P.; Pidcock, E.; Rodriguez-Monge, L.; Taylor, R.; van de Streek, J. and Wood, P. A. *J. Appl. Cryst.*, **2008**, *41*, 466-470

[9] A. L. Spek, *Acta Cryst*. **2009**, *D65*, 148.

[10] a) F. Neese, *WIREs Comput Mol Sci* **2012**, *2*, 73; b) F. Neese, *WIREs Comput Mol Sci* **2022**, *12*, e1606.

[11] S. Grimme, A. Hansen, S. Ehlert, J.-M. Mewes, *J. Chem. Phys.* **2021**, *154*, 064103

[12] a) M. Bursch, H. Neugebauer, S. Ehlert, S. Grimme, *J. Chem. Phys.* **2022**, *156*, 134105; b) E. Caldeweyher, S. Ehlert, A. Hansen, H. Neugebauer, S. Spicher, C. Bannwarth, S. Grimme, *J. Chem. Phys.* **2019**, *150*, 154122; c) J. Zheng, X. Xu, D. G. Truhlar, *Theor. Chem. Acc.* **2011**, *128*, 295; d) A. V. Marenich, C. J. Cramer, D. G. Truhlar, *J. Phys. Chem. B* **2009**, *113*, 6378.

[13] J. N. Harvey, F. Himo, F. Maseras, L. Perrin, *ACS Catal.* **2019**, *9*, 6803.

[14] NBO 7.0. E. D. Glendening, J. K. Badenhoop, A. E. Reed, J. E. Carpenter, J. A. Bohmann, C. M. Morales, P. Karafiloglou, C. R. Landis, and F. Weinhold, Theoretical Chemistry Institute, University of Wisconsin, Madison, WI (2018),

[15] AIMAll (Version 19.10.12), Todd A. Keith, TK Gristmill Software, Overland Park KS, USA, 2019 (Aim.Tkgristmill.Com)